Space Weather

RESEARCH ARTICLE
10.1029/2018SW002077

One- to 10-Day Forecasts of Ionospheric Total Electron Content Using a Statistical Model

J. L. Lean[1]

[1]Space Science Division, Naval Research Laboratory, Washington, DC, USA

Key Points:
- A statistical model is used to forecast TEC on time scales longer than 1 day
- The average over the globe of the mean absolute error of 5-day forecasts is 2.7 TECU; averaged over 30°S to 30°N, it is 3.5 TECU
- Forecast skill is highest in April, when 5-day TEC forecasts averaged over the globe exceed persistence by ~16% and climatology by ~21%

Supporting Information:
- Supporting information S1
- Data Set S1
- Data Set S2
- Data Set S3
- Data Set S4
- Data Set S5
- Data Set S6

Correspondence to:
J. L. Lean,
judith.lean@nrl.navy.mil

Citation:
Lean, J. L. (2019). One- to 10-day forecasts of ionospheric total electron content using a statistical model. *Space Weather*, *17*, 313–338. https://doi.org/10.1029/2018SW002077

Received 11 SEP 2018
Accepted 22 JAN 2019
Accepted article online 29 JAN 2019
Published online 23 FEB 2019

Abstract A new, rapid, nonassimilative technique is demonstrated for forecasting the ionosphere's vertical total electron content (TEC) on time scales longer than 1 day. The approach uses a statistical model constructed by regressing solar extreme ultraviolet irradiance and seasonal, diurnal, and geomagnetic predictors at multiple lags against the 2-hourly International Global Navigation Satellite Systems Service observations, with a formulation that accounts for solar modulation of the seasonal oscillations and solar and seasonal modulation of the diurnal oscillations. Solar irradiance inputs to the statistical model are forecast at successive 2-hr intervals from 1999 to 2015 using an autoregressive model of irradiance variations during the prior 100 days. As the forecast time increment increases from 1 to 10 days, the average over the globe of the mean absolute error of TEC observations and the forecasts increases from 2.5 to 3.2 TECU (total electron content unit, 1 TECU = 10^{16} el/m^2); the root-mean-square error increases from 3.7 to 4.8 TECU. Averaged over the equatorial ionization anomaly region (30°S–30°N) the mean absolute error of the forecasts increases from 3.2 to 4.3 TECU and the root-mean-square error increases from 4.6 to 6.4 TECU. The skill of the TEC forecasts at time increments of 3, 5, and 8 days ahead exceeds persistence by 9%, 13%, and 15% and climatology by 9%, 12%, and 10%, respectively. Forecast skill is higher in April than in July. Long-range, multiyear forecasts from 2018 to 2030 are demonstrated based on current expectations that solar activity in cycle 25 will be comparable to that in cycle 24.

1. Introduction

Forecasting the future state of the ionosphere is a fundamental challenge for near-space environment research and operations. The U.S. National Space Weather Action Plan (SWAP, 2015) identifies one of six overall goals as "Improve Space-Weather Services through Advancing Understanding and Forecasting". In pursuit of this goal, the Space Weather Phase I Benchmarks (2017) cites the need for improvements in forecasting lead time and accuracy, enhanced fundamental understanding of space weather and its drivers, and improved predictive models, including of total electron content (TEC, defined such that 1 TECU [total electron content unit, 1 TECU = 10^{16} el/m^2] is the number of electrons in a column of 1 m^2 cross-sectional area), especially during geomagnetic disturbances. Reliable specification and forecasting of TEC can help mitigate uncertainties in precision timing and navigation (Filler et al., 2004), which impede space situational awareness, single-band high-frequency radio operations, and satellite geolocation, with attendant societal and military consequences (American Meteorological Society, 2011; Cannon, 2009).

Ionospheric TEC varies on time scales from minutes to decades as a result of geographically dependent responses of the ionosphere and thermosphere to a range of different influences, primarily from the Sun. Changes in the amount of solar extreme ultraviolet (EUV) radiation as the Earth spins and orbits the Sun produce dominant diurnal and seasonal cycles. Intrinsic changes in solar EUV irradiance associated with the Sun's rotation and changing magnetic activity produce additional cycles of approximately 27 days and 11 years. On shorter time scales of hours to days, eruptive events on the Sun can propel coronal mass ejections to Earth, altering geomagnetic activity and producing rapid and potentially large regional and vertical redistributions of the extant electron density, itself dependent on the incoming solar radiation at a given local time, season, and location (Fuller-Rowell et al., 2000; Wood et al., 2016).

The total number of electrons in the ionosphere determines the time for radio waves to travel between earth-orbiting spacecraft and ground-based receivers. Unspecified fluctuations in total electron density translate to errors in transit time and distance such that an uncertainty of 1 TECU corresponds to a range error of 16.24 cm for the Global Positioning Satellite (GPS) L1 frequency 1,575.42 MHz (Jakowski et al., 2011). Natural TEC variations in response to changes in incoming solar radiation are much larger than 1 TECU.

Diurnal changes, for example, exceed 100 TECU in equatorial regions (e.g., Hawaii) during high solar activity and are tens of TECU at high latitudes (e.g., Weddell Sea). Diurnal cycles are themselves superimposed on annual and semiannual oscillations (AO and SAO) with amplitudes that range from tens of TECU at high solar activity to a few TECU during solar minima (Lean et al., 2016).

Current space weather operations provide near-real-time specification and 24-hr forecasts of ionospheric parameters, including TEC, by using ionospheric observations to adjust initial model-based specifications. The US-TEC capability of the Space Weather Prediction Center (SWPC), for example, assimilates data into an empirical model of TEC over the continental United States (Fuller-Rowell et al., 2006); estimated uncertainties in real-time specification are 2 TECU during quiet geomagnetic conditions. The Global Assimilative Ionosphere Model (GAIM) ingests multiple observations to specify total and vertical profiles of low-latitude and midlatitude electron density (from 60°S to 60°N) in support of Air Force operations (Schunk et al., 2014); GAIM's 24-hr forecasts assume persistence of the diurnal cycle unaltered by either solar irradiance or geomagnetic activity. The European Digital Upper Atmosphere Server uses ground-based observations to specify electron density peak heights and concentrations over Europe (Belehaki et al., 2006). Twenty-four-hour forecasts incorporating models of solar wind impacts to estimate prospective geomagnetic influences demonstrate improved forecast skill relative to persistence and climatology (Tsagouri, 2011; Tsagouri et al., 2018).

There are, as yet, no operational forecasts of ionospheric TEC beyond 24 hr. Indeed, it is argued that meaningful forecasts longer than a day or so ultimately require the use of coupled global-scale physical models to account for the multiple processes that facilitate the ionosphere's complex responses to changing solar and geomagnetic inputs to the Earth system (Mannucci et al., 2015; Schunk et al., 2012). Such a capability is, however, deemed insufficiently mature for operational application. With the goal of assessing current capability and identifying needed improvements in TEC specification, a recent community-wide "challenge" quantified differences from observations of eight ionospheric models during the December 2006 storm event; the root-mean-square error (RMSE) ranged from 3 TECU at high latitudes to 13 TECU at low latitudes (Shim et al., 2017).

Whatever the approach used to specify and forecast the ionosphere, metrics are crucial for comparing different techniques and providing a baseline against which to measure future progress (Shim et al., 2017; Tsagouri, 2011). This paper assesses the capability of a statistical model to forecast vertical TEC at all geographical locations (on a 72×71 longitude-latitude grid) more than 1 day ahead. Whereas the persistence of the diurnal cycle in TEC at a given location is the basis for forecasts less than 24 hr, on longer time scales of days to months, both seasonal and solar cycles produce additional ionospheric variability. Given the solar EUV irradiance and geomagnetic inputs for a particular time and day of year, the statistical model estimates the corresponding TEC from parametrizations of the solar, seasonal, diurnal, and geomagnetic influences detected in 17 years of TEC observations; near-real-time ionospheric observations are not needed. As such, the approach provides a baseline against which to quantify advances in forecasting capabilities on longer time scales, including extensions of current assimilative approaches.

Following an overview of the database of TEC observations derived from GPS signals and the statistical model of TEC variability constructed from this database, section 2 quantifies the model performance during 1999 to 2015, the time period of estimation of the model parameters, and from 2016 to 2017 to independently validate the model's performance using observations that were not used in the model's construction. The specific metrics of model performance used are the RMSE, mean absolute error (MAE), and mean absolute percentage error (MAPE) of the model and observations; the TEC observations used are the official product of the GPS International Global Navigation Satellite Systems (GNSS) Service (IGS) Ionosphere Working Group (Hernández-Pajares et al., 2009). Section 3 develops and applies the forecast technique, determines the RMSE, MAE, and MAPE metrics of the model's 1- to 10-day forecasts, and evaluates the skill of the model forecasts relative to forecasts made using persistence and climatology. Section 4 discusses the statistical model's forecast capability and illustrates the plausibility of longer-range forecasts. Section 4 also investigates the statistical model's ability to specify TEC disruptions by geomagnetic activity (which were not included in the forecasts) by comparing the model's specification of TEC during the December 2006 storm event with the community challenge results (Shim et al., 2017). Section 5 summarizes the 1- to 10-day forecast capability of the statistical model.

2. Statistical Model of TEC Variability

2.1. IGS TEC Database

The IGS Ionosphere Working Group produces a database of geographical maps of vertical TEC derived from GPS data (Hernández-Pajares et al., 2009). The IGS TEC maps, each with 72 (longitude) × 71 (latitude) bins and available at 2-hr intervals since mid-1998, are weighted means of maps produced at four GPS analysis centers. As an official product of the IGS Working Group on the Ionosphere, the IGS TEC maps have been tested and validated and are considered superior to any of the databases of TEC maps from individual centers. Weekly comparisons of the slant TEC for a small set of permanent IGS stations and external self-consistency checks validate the weighting scheme. TOPEX altimeter data provide routine validation of the TEC maps after July 2001. Figure 1a shows the time series of globally averaged 2-hr values obtained by summing over the longitude and latitude bins of each IGS TEC map, accounting for the (cosine latitude) area factor.

An important aspect of GPS-derived TEC observations that contributes to uncertainties in the IGS database is that TEC is derived from ground-based GPS receivers that are deployed primarily in the continental Northern Hemisphere, with a lack of receivers over oceans and in the Southern Hemisphere (Hernández-Pajares et al., 2009; Jee et al., 2010). As well, the measured quantity is the TEC in a slant column between the spacecraft and ground receiver, requiring algorithmic conversion to vertical TEC; the four analysis centers perform this conversion independently using different approaches.

Biases in absolute TEC among individual analyses are in the range 1 to 3 TECU (Hernández-Pajares et al., 2009). Consistent with this, comparisons of the IGS TEC database with the independent Massachusetts Institute of Technology TEC database suggest an average error of 2 TECU (Shim et al., 2017). Comparisons of GPS-derived vertical TEC with direct altimeter data over oceans (where GPS receivers are lacking) from the end of 2002 to the end of 2007 suggest that the upper bound of IGS TEC relative error is 20% (Hernández-Pajares et al., 2009). A more extensive comparison of TEC from 1998 to 2009 found that GPS-derived TEC products reproduce the spatial and temporal variations in altimeter data globally and seasonally quite well but not the detailed structure in equatorial regions and the Weddell Sea (Jee et al., 2010). That study suggested that the current network of GPS ground receivers imposes fundamental limitations on deriving vertical TEC at high northern latitudes and at southern middle and high latitudes, where differences from direct altimeter data can reach 50% or more, especially when solar activity is low.

2.2. Statistical Model Description

A statistical model of TEC variability constructed using the IGS TEC observations from 1998 to 2015 specifies 2-hourly TEC as functions of solar EUV irradiance, seasonal (annual, semiannual, terannual, and biennial) and diurnal (diurnal, semidiurnal, and terdiurnal) oscillations and geomagnetic activity; solar activity modulates the seasonal oscillations, and both solar activity and the seasonal oscillations modulate the diurnal oscillations. Lean et al. (2016) provide details of the model formulation and describe regional response patterns of TEC to individual variability components. The model, TEC_{mod}, estimates the observed ionospheric TEC, TEC_{obs}, at Universal Time (UT), t, at a specified longitude, $\varnothing$, and latitude, λ, as

$$TEC_{\mathrm{obs}}(\varnothing,\lambda,t) = TEC_{\mathrm{mod}}(\varnothing,\lambda,t) + R(\varnothing,\lambda,t) \tag{1}$$

where R is the residual error, that is, temporal variability in TEC observations at each longitude and latitude that the model does not capture. The corresponding globally integrated quantities are

$$TEC_{\mathrm{obs}}^{\mathrm{glob}}(t) = TEC_{\mathrm{mod}}^{\mathrm{glob}}(t) + R^{\mathrm{glob}}(t) \tag{2}$$

Specifically, the model adds to the baseline (invariant) TEC, TEC_0 ($\varnothing$, λ), variations arising from solar activity, $\Delta TEC_{\mathrm{sol}}$ ($\varnothing$, λ,t), seasonal oscillations, $\Delta TEC_{\mathrm{seas}}$($\varnothing$, λ, t), diurnal oscillations, $\Delta TEC_{\mathrm{diur}}$($\varnothing$, λ,t) and geomagnetic activity, $\Delta TEC_{\mathrm{geo}}$($\varnothing$, λ, t), such that

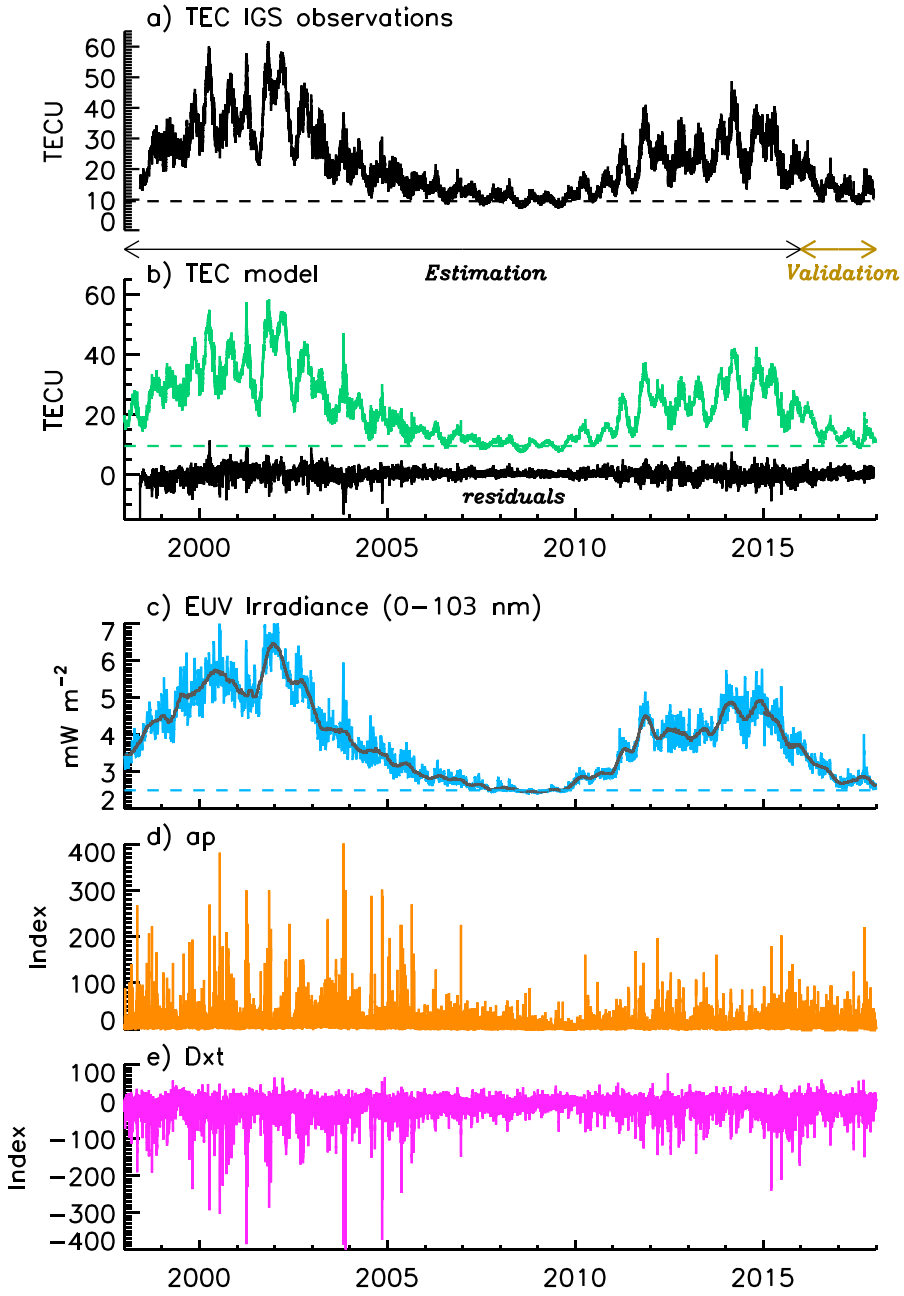

Figure 1. (a) The International Global Navigation Satellite Systems Service (IGS) 2-hourly observations of global TEC from mid-1998 to the end of 2017. (b) The statistical model of global TEC variability reproduces the observations with residuals that have a mean absolute error of 1.1 TECU and root-mean-square error of 1.6 TECU. The statistical model calculates TEC using as inputs (c) the Sun's total EUV irradiance (at wavelengths less than 103 nm) and the geomagnetic (d) *ap* and (e) *Dxt* indices. The statistical model is constructed from observations in the estimation period (1998 to 2015). The subsequent two years (2016 and 2017) provide independent validation of the model using observations not included in its formulation. TEC = total electron content; TECU = TEC unit, 1 TECU = 10^{16} el/m^2; EUV = extreme ultraviolet.

$$TEC_{\mathrm{mod}}(\varnothing,\lambda,t) = TEC_0(\varnothing,\lambda) + \Delta TEC_{\mathrm{sol}}(\varnothing,\lambda,t) + \Delta TEC_{\mathrm{seas}}(\varnothing,\lambda,t) + \Delta TEC_{\mathrm{diur}}(\varnothing,\lambda,t) + \Delta TEC_{\mathrm{geo}}(\varnothing,\lambda,t) \quad (3)$$

The absolute scale of the model's TEC is that of the IGS database used to construct the model. As such, the TEC of the baseline (invariant) ionosphere, TEC_0 ($\varnothing$, λ), has a global value $\Sigma TEC_0(\varnothing, \lambda)\cos(\lambda)/72\Sigma\cos(\lambda) = 9.5$ TECU.

The statistical model specifies the solar-induced change in TEC, $\Delta TEC_{\mathrm{sol}}$, using values of solar EUV irradiance summed over wavelengths less than 103 nm, $E(t)$, at $n_{\mathrm{sol}} = 11$ lags according to

$$\Delta TEC_{\mathrm{sol}}(\varnothing,\lambda,t) = \sum_{n=1}^{n_{\mathrm{sol}}} a_n(\varnothing,\lambda)[E(t-\tau_n)-E_{\mathrm{min}}] \tag{4}$$

where E_{min} is the value of E at solar activity minimum and $E(t-\tau_n)$ is the EUV irradiance at a lag of τ_n days, for lags at 0, 0.5, 1, 1.5, 2, 3, 4, 6, 8, 24, and 36 days. A model of irradiance variability developed from observations made by the Solar EUV Experiment on the Thermosphere Ionosphere Mesosphere Energetic and Dynamics spacecraft specifies the daily solar EUV irradiance in terms of the Mg core-to-wing ratio and the 10.7 cm radio flux (Lean, Woods, et al., 2011).

A combination of baseline (invariant) and solar-modulated sine and cosine functions at four periods, P_{seas}, at 121.7, 182.6, 365.25, and 730.5 days, specifies seasonal TEC variability in the model, as

$$\begin{aligned}\Delta TEC_{\mathrm{seas}}(\varnothing,\lambda,t) = &\sum_{n=1}^{n_{\mathrm{seas}}}\left[b_n(\varnothing,\lambda)\sin\left(\frac{2\pi t}{P_{\mathrm{seas}}(n)}\right)+c_n(\varnothing,\lambda)\cos\left(\frac{2\pi t}{P_{\mathrm{seas}}(n)}\right)\right]\\ &+\sum_{n=1}^{n_{\mathrm{seas}}}\left[d_n(\varnothing,\lambda)\sin\left(\frac{2\pi t}{P_{\mathrm{seas}}(n)}\right)+e_n(\varnothing,\lambda)\cos\left(\frac{2\pi t}{P_{\mathrm{seas}}(n)}\right)\right]\times\left[E^{81}(t)-E^{81}_{\mathrm{min}}\right]\end{aligned} \tag{5}$$

where $n_{\mathrm{seas}} = 4$ are the four periods of the seasonal oscillations and the sine and cosine terms permit determination of both the phase and amplitude of each. Amplitude modulation is prescribed as a linear function of the 81-day smoothed solar EUV irradiance $E^{81}(t)$ relative to its solar minimum value, E^{81}_{min}.The periods 182.6 and 365.25 days correspond to the SAO and AO, the two largest peaks in the periodogram of daily averaged global TEC. The periods 121.7 and 730.5 days correspond to smaller-amplitude terannual and biennial oscillations that are present in the residuals of the TEC data and in an initial model constructed with only the SAO and AO cycles (Lean, Meier, et al., 2011).

To account for the modulation of TEC throughout the day by Earth's rotation and orbit, which alter the subsolar geographical location of incident solar EUV radiation, the statistical model includes $n_{\mathrm{diurn}} = 3$ cycles with periods, P_{diurn}, at 0.33, 0.5, and 1 days. Both solar activity and the seasonal oscillations modulate the three diurnal cycles, so that

$$\begin{aligned}\Delta TEC_{\mathrm{diur}}(\varnothing,\lambda,\mathrm{t}) = &\sum_{n=1}^{n_{\mathrm{diur}}} f_n(\varnothing,\lambda)\sin\left(\frac{2\pi t}{P_{\mathrm{diur}}(n)}\right)+g_n(\varnothing,\lambda)\cos\left(\frac{2\pi t}{P_{\mathrm{diur}}(n)}\right)\\ &+\sum_{n=1}^{n_{\mathrm{diur}}}\left[h_n(\varnothing,\lambda)\sin\left(\frac{2\pi t}{P_{\mathrm{diur}}(n)}\right)+i_n(\varnothing,\lambda)\cos\left(\frac{2\pi t}{P_{\mathrm{diur}}(n)}\right)\right]\times\left[E^{81}(t)-E^{81}_{\mathrm{min}}\right]\\ &+\sum_{n=1}^{n_{\mathrm{diur}}}\sum_{m=1}^{n_{\mathrm{seas}}}\left[j_{nm}(\varnothing,\lambda)\sin\left(\frac{2\pi t}{P_{\mathrm{diur}}(n)}\right)\times\sin\left(\frac{2\pi t}{P_{\mathrm{seas}}(m)}\right)+k_{nm}(\varnothing,\lambda)\right.\\ &\sin\left(\frac{2\pi t}{P_{\mathrm{diur}}(n)}\right)\times\cos\left(\frac{2\pi t}{P_{\mathrm{seas}}(m)}\right)+l_{nm}(\varnothing,\lambda)\cos\left(\frac{2\pi t}{P_{\mathrm{diur}}(n)}\right)\times\sin\left(\frac{2\pi t}{P_{\mathrm{seas}}(m)}\right)\\ &\left.+m_{nm}(\varnothing,\lambda)\cos\left(\frac{2\pi t}{P_{\mathrm{diur}}(n)}\right)\times\cos\left(\frac{2\pi t}{P_{\mathrm{seas}}(m)}\right)\right]\\ &+\sum_{n=1}^{n_{\mathrm{diur}}}\sum_{m=1}^{n_{\mathrm{seas}}}\left[n_{nm}(\varnothing,\lambda)\sin\left(\frac{2\pi t}{P_{\mathrm{diur}}(n)}\right)\times\sin\left(\frac{2\pi t}{P_{\mathrm{seas}}(m)}\right)\right.\\ &+o_{nm}(\varnothing,\lambda)\sin\left(\frac{2\pi t}{P_{\mathrm{diur}}(n)}\right)\times\cos\left(\frac{2\pi t}{P_{\mathrm{seas}}(m)}\right)+p_{nm}(\varnothing,\lambda)\cos\left(\frac{2\pi t}{P_{\mathrm{diur}}(n)}\right)\times\\ &\left.\sin\left(\frac{2\pi t}{P_{\mathrm{seas}}(m)}\right)+q_{nm}(\varnothing,\lambda)\cos\left(\frac{2\pi t}{P_{\mathrm{diur}}(n)}\right)\times\cos\left(\frac{2\pi t}{P_{\mathrm{seas}}(m)}\right)\right]\times\left[E^{81}(t)-E^{81}_{\mathrm{min}}\right]\end{aligned} \tag{6}$$

The statistical model represents changes in TEC, $\Delta TEC_{\mathrm{geo}}$, during ionospheric storms in response to eruptive solar events using the 3-hr *ap* index obtained from the U.S. National Geophysical Data Center, lagged 0 and 0.5 days, and the *Dxt* index provided by the University of Oulu, Finland, lagged 1 day. Specifically,

$$\Delta TEC_{\text{geo}}(\varnothing,\lambda,t) = \sum_{n=1}^{n=2} r_n(\varnothing,\lambda)ap(t-\tau_n) + r_3(\varnothing,\lambda)Dxt(t-\tau_3) \quad (7)$$

The *ap* index is an indicator of the general level of geomagnetic activity over the globe, derived from ground-based magnetometers. The *Dxt* index is based on the average value of the horizontal component of the Earth's magnetic field measured at four near-equatorial geomagnetic observatories (e.g., Verbanac et al., 2010). The three different lags in the statistical model accommodate an initial ionospheric positive response to geomagnetic activity within the first day after arrival of a coronal mass ejection at earth and a subsequent negative phase beginning a day or so later (Mendillo, 2006; Wood et al., 2016). In reality, solar activity and the seasonal and diurnal oscillations modulate to some extent the TEC response to geomagnetic activity, since these longer time scale influences determine the overall level of ionospheric plasma upon which the geomagnetic disturbance processes act (Mendillo, 2006). The present model, however, does not include these additional modulated terms.

Multiple linear regression of the solar, seasonal, diurnal, and geomagnetic predictors against observed TEC during the period mid-1998 to 2015 estimates the model's 139 coefficients, using linear least squares fitting to minimize the sum of squares of the residuals, $R(t)$, of the model and observations. Since the model is constructed at each longitude and latitude grid point (and separately for global TEC), the derived coefficients at each latitude and longitude directly map the regional patterns of the individual responses. Lean et al. (2016) describe and interpret these patterns of spatial TEC variability.

For a given day of the year, time of day, solar EUV irradiance at 11 specified lags, the geomagnetic *ap* index at two lags, and the *Dxt* index at one lag, the statistical model calculates TEC_{mod} as an estimate of the observed TEC_{obs} at a specified longitude, $\varnothing$, and latitude, λ, according to equation (3). Figure 1 compares the model of global TEC with the IGS observations from 1998 to 2017 and shows the residuals of the observations and model; the correlation of the model with the observations is 0.99, and the standard deviation of the residuals is 1.6 TECU. The standard deviation of the model and observations averaged over all longitudes and latitudes is 3.5 TECU. Also shown in Figure 1 are the model's EUV irradiance and geomagnetic predictors.

2.3. Model Performance, Estimation Period (1998–2015)

The model's performance in the estimation period provides a baseline against which to assess its performance in the subsequent validation period and the forecasts. Metrics of a model's performance relative to n observations include (von Storch & Zwiers, 1999; Wilks, 1995) the RMSE, MAE, and MAPE. These quantifies are determined numerically as

$$RMSE = \sqrt{\frac{1}{n}\sum_{k=1}^{n}\left(TEC_{\text{mod}_k} - TEC_{\text{obs}_k}\right)^2} \quad (8)$$

$$MAE = \frac{1}{n}\sum_{k=1}^{n}\left|TEC_{\text{mod}_k} - TEC_{\text{obs}_k}\right| \quad (9)$$

$$MAPE = \frac{100}{n}\sum_{k=1}^{n}\left(\frac{\left|TEC_{\text{mod}_k} - TEC_{\text{obs}_k}\right|}{TEC_{\text{obs}_k}}\right) \quad (10)$$

where $TEC_{\text{mod}} - TEC_{\text{obs}}$ are the model-observation residuals, R (equation (1)).

Although the RMSE is widely used as a metric for assessing model performance (e.g, Shim et al., 2017), the MAE is arguably preferable for quantifying differences of modeled and observed TEC. This is because positional range error depends directly on the number of electrons (in TECU) between a radio frequency emitter and receiver. Whereas the MAE simply averages the absolute model-observation residuals, the RMSE depends not just on the magnitude of the residuals but also on "the distribution of error magnitudes (or squared errors) and $n^{1/2}$" (the square root of the number of residuals). For this reason, Willmott and Matsuura (2005) argue that for assessing average model performance the MAE is superior to the RMSE, but Chai and Draxler (2014) question the superiority of MAE over RMSE, noting that a combination of metrics is "often required to assess model performance".

Table 1 therefore lists numerical values for multiple metrics of model performance, specifically the RMSE, MAE, and MAPE of the residuals of the statistical model and observations averaged over all latitudes and

Table 1
Metrics of the Performance of the Statistical Model Specification of Regional TEC Averaged Over the Globe and, in Parenthesis, of Global TEC, at Different Levels of Solar Activity, Estimated Using All 2-Hourly Values on All Days of the Specified Time Intervals and Months

	1998–2015	2000–2001	2005–2006	2008–2009	2016–2017
Parameter	Model estimation period	High solar activity	Similar solar activity as model validation	Low solar activity	Model validation period
EUV irradiance (mW/m^2)					
Daily	3.92	5.51	2.97	2.52	2.96
81-day mean	3.92	5.52	2.97	2.52	2.96
F10.7 cm flux	118.4	180.6	85.9	69.8	83.0
ap index	10.6	14.0	11.0	5.4	10.5
Dxt index	−12.1	−17.8	−12.5	−6.2	−15.7
TEC (TECU)	22.8	38.2	14.3	10.1	14.1
Correlation with observations	0.96 (0.99)	0.93 (0.97)	0.95 (0.94)	0.96 (0.92)	0.94 (0.95)
Root-mean-square error (RMSE, TECU)					
All months	3.6 (1.6)	5.1 (2.3)	2..0 (0.9)	1.3 (0.6)	2.3 (1.1)
April	4.0 (2.0)	6.4 (3.9)	2.2 (0.9)	1.4 (0.6)	2.7 (1.7)
July	2.6 (1.3)	3.9 (2.0)	1.7 (0.7)	0.9 (0.4)	1.8 (0.8)
Mean absolute error (MAE, TECU)					
All months	2.4 (1.2)	3.7 (1.8)	1.4 (0.7)	0.9 (0.4)	1.7 (0.8)
April	2.7 (1.4)	4.8 (3.0)	1.6 (0.7)	1.0 (0.5)	2.1 (1.4)
July	1.8 (0.9)	2.8 (1.6)	1.2 (0.5)	0.7 (0.3)	1.4 (0.6)
Mean absolute percentage error (MAPE, %)					
All months	16 (15)	13 (11)	14 (13)	13 (11)	20 (22)
April	16 (17)	15 (15)	14 (13)	13 (12)	24 (39)
July	17 (26)	14 (20)	15 (19)	12 (18)	23 (31)

Note. The averages over the globe are numerical averages of the metrics of the performance of the regional statistical model constructed using equation (3) at each of the model's 72 × 71 longitude-latitude grid points. The global TEC metrics pertain to the performance of a separate statistical model of global TEC. EUV = extreme ultraviolet; TEC = total electron content; TECU = TEC unit, 1 TECU = 10^{16} el/m^2.

longitudes and for global TEC (in parenthesis). The performance metrics are calculated for the entire estimation period (1998–2015) and for subepochs of relatively high (2000–2001), moderate-to-low (2005–2006), and low (2008–2009) solar activity. Table 1 also lists the average values of solar EUV irradiance, geomagnetic activity, and TEC during the individual epochs. Figure 2 shows the corresponding regional distributions of the performance metrics (whose average values are those listed in Table 1) during the entire estimation period (on the left) and for 2 years of relatively high solar activity (on the right). The metrics are the correlation coefficient of the model and observations (Figures 2a and 2e), the RMSE (Figures 2b and 2f), MAE (Figures 2c and 2g), and MAPE (Figures 2d and 2h).

Maximum differences between the model and observations occur at low latitudes (30–30°S) in the equatorial ionization anomaly (EIA) region. During the estimation period, the maximum regional RMSE (Figure 2b) is 6.7 TECU (e.g., near Hawaii), and 2.7% of low-latitude grid points (49 of 1,800) have RMSE between 6 and 6.7 TECU. The maximum regional MAE (Figure 2c) is 4.6 TECU, and 4.6% low-latitude locations (82 of 1,800) have MAE between 4 and 4.6 TECU. At latitudes higher than 30° the model specifies TEC with RMSE < 5 TECU and MAE < 3.3 TECU. Since absolute values of TEC maximize at low latitudes and become increasingly smaller at higher latitudes (see, e.g., Lean et al., 2016, Figure 1) the regional pattern of the model performance in terms of percentage, MAPE (Figure 2d), differs from the (similar) RMSE and MAE patterns. MAPE is less than 19% at all northern latitudes and at southern latitudes lower than 30°; MAPE of up to 31% occur at high southern latitudes.

The performance metrics in Table 1 and Figure 2 demonstrate that when solar activity is higher than average, the RMSE and MAE of the statistical model and observations increase (Figures 2f and 2g) and the MAPE decreases (Figure 2h) because TEC values are overall higher. Whereas the MAE averaged over the globe for the entire estimation period is 2.4 TECU, it increases to 3.7 TECU during higher solar (2000–2001) and

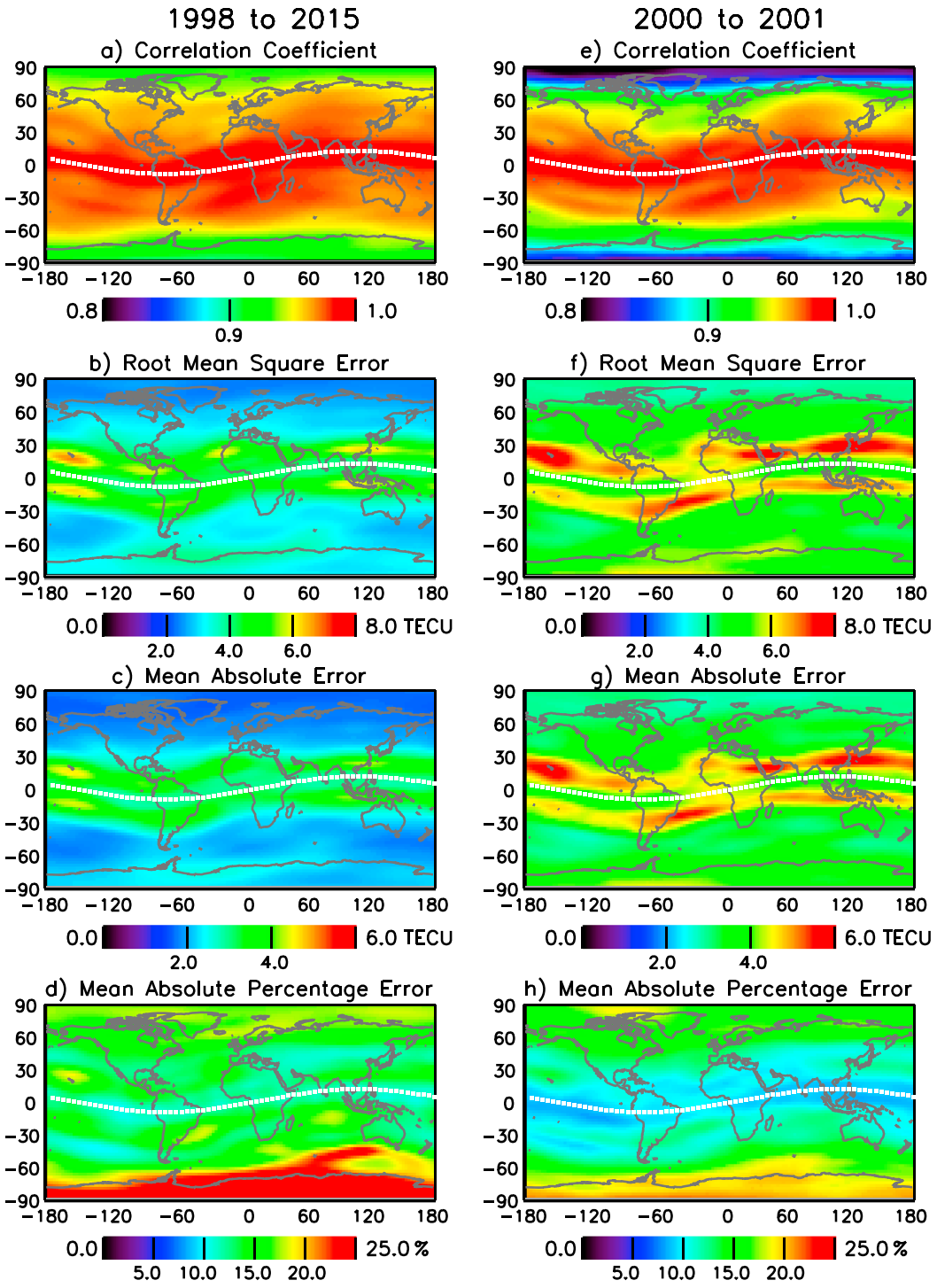

Figure 2. Metrics of the statistical model's performance relative to International Global Navigation Satellite Systems Service TEC observations are shown regionally during the 17-year estimation period, including (a) the correlation of the model and observations, (b) the root-mean-square error (RMSE), (c) the mean absolute error (MAE), and (d) the mean absolute percentage error (MAPE). The metrics (e) correlation coefficient, (f) RMSE, (g) MAE, and (h) MAPE are determined separately for a 2-year period of high solar activity (2000 and 2001). TECU = total electron content unit, 1 TECU = 10^{16} el/m^2.

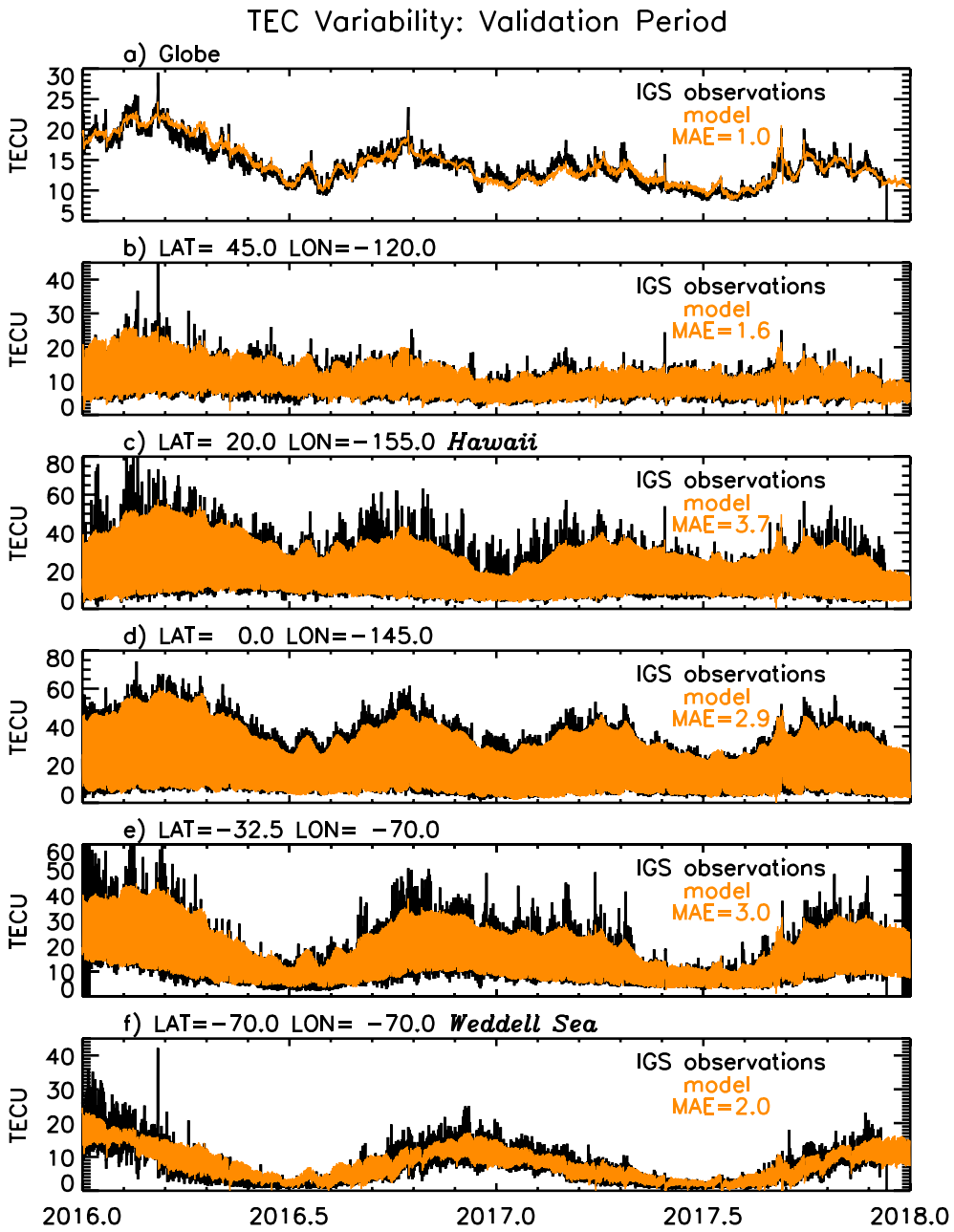

Figure 3. Compared with the IGS observation during 2016 and 2017 are (a) global TEC and (b, c, d, e, and f) TEC at various geographical locations estimated using the statistical model constructed with observations in the estimation period (1998–2015) and the EUV and geomagnetic inputs shown in Figure 1 during the validation period. IGS = International Global Navigation Satellite Systems Service; TEC = total electron content; TECU = TEC unit, 1 TECU = 10^{16} el/m^2; EUV = extreme ultraviolet.

decreases to 0.9 TECU during solar minimum (2008–2009). In addition to depending on location and solar activity, the statistical model's ability to specify TEC also depends on season; the MAE of the observations and model averaged over the globe (for the entire estimation period) is 2.7 TECU in April and 1.8 TECU in July.

2.4. Model Performance, Validation Period (2016–2017)

Specification of TEC during the period 2016–2017 enables independent validation of the statistical model's performance using observations that are not included in the regression that determines the model

coefficients. As Figure 1 shows, the time period of model validation is shorter than the estimation period (2 instead of 17 years) and TEC absolute values are lower overall than on average because solar activity is lower, nearing the approach to solar minimum conditions. Table 1 lists average values of solar EUV irradiance, geomagnetic activity, and TEC during the validation period for comparison with the estimation period.

Figure 3 illustrates the observed and modeled values of TEC during 2016 and 2017, globally (Figure 3a) and at separate locations spanning a range of latitudes, including Hawaii (Figure 3c) and the Weddell Sea (Figure 3f). The modeled values are specified using the solar EUV irradiance and geomagnetic activity shown in Figure 1 for the validation period. Figure 4 shows regional distributions of model performance in the 2-year validation period (analogously to those in Figure 2 for the estimation period), specifically the correlation coefficient of the model and observations (Figure 4a), and the RMSE (Figure 4b), MAE (Figure 4c), and MAPE (Figure 4d) of the residuals. To more appropriately compare the performance of the model in the validation and estimation periods, Figure 4 also shows performance metrics for the 2-year interval 2005 to 2006 (in the estimation period) for which, as Figure 1 shows, solar activity levels and global TEC values are comparable to those of the validation period (Table 1).

During the 2-year validation period average solar and geomagnetic activity are both smaller than the average over the entire estimation period but larger than during solar minimum (Table 1). As expected, the average over the globe of the RMSE and MAE of the TEC model and observations in the validation period (RMSE = 2.3 TECU, MAE = 1.7 TECU) are likewise smaller than during the entire estimation period (RMSE = 3.6 TECU, MAE = 2.4 TECU) but larger than during solar minimum (RMSE = 1.3 TECU, MAE = 0.9 TECU). As well, the patterns of the regional performance metrics during the validation period are similar to those in the estimation period; the highest values of RMSE and MAE occur at similar low-latitude sites in the EIA, the lowest values at high latitudes and the highest MAPE in the Antarctic region (Figures 2 and 4). These comparisons suggest that the model's performance during the validation period is consistent overall with its performance in the estimation period. However the metrics averaged over the globe in the validation period (RMSE = 2.3 TECU, MAE = 1.7 TECU) are somewhat larger than during 2005–2006 (RMSE = 2.0 TECU, MAE = 1.4 TECU) for which solar activity and geomagnetic activity are comparable (but not identical). Whether these differences indicate a degradation of model performance in the validation period (relative to the estimation period) or are the result of modest, but real, differences in solar and geophysical conditions is unclear because the period 2016–2017 is too short to provide unequivocal validation.

3. Model Forecasts

The statistical model represents variations in TEC in terms solar, geomagnetic, seasonal, and diurnal predictors, using multiple linear regression to establish the model coefficients (equations (3)–(7)). With the model coefficients (a_n, b_n ... $.r_n$) determined using TEC observations from 1998 to 2015, a forecast of TEC at any time (past, present, or future) is possible providing the model inputs are known or estimated at that time. For forecasting TEC on time scales of 1 to 10 days ahead, this requires forecasting solar EUV irradiance and geomagnetic activity (using past and current observations, either of the indices themselves, or other relevant geophysical quantities) which alter TEC directly and also modulate the seasonal and diurnal oscillations. The sine and cosine functions that represent the seasonal and diurnal changes (equations (5) and (6)) are explicit functions of time and depend also on the smoothed EUV irradiance (which on time scales of 1 to 10 days varies only minimally) and so are readily propagated forward or backward.

Specifying t_0 as the time at which a forecast is made and Δt as the time increment after t_o for which the TEC is forecast, the model forecasts ionospheric TEC, TEC_{fc} at a specified longitude, $\varnothing$, latitude, λ, and time, $t_0 + \Delta t$, using equation (3), as

$$TEC_{fc}(\varnothing,\lambda,t_0+\Delta t) = TEC_0(\varnothing,\lambda) + \Delta TEC_{\mathrm{sol}}(\varnothing,\lambda,t_0+\Delta t) + \Delta TEC_{\mathrm{seas}}(\varnothing,\lambda,t_0+\Delta t) + \Delta TEC_{\mathrm{diur}}(\varnothing,\lambda,t_0+\Delta t) + \Delta TEC_{\mathrm{geo}}(\varnothing,\lambda,t_0+\Delta t) \quad (11)$$

where equations (4)–(7) provide the numerical expressions of the individual components. The ability of the

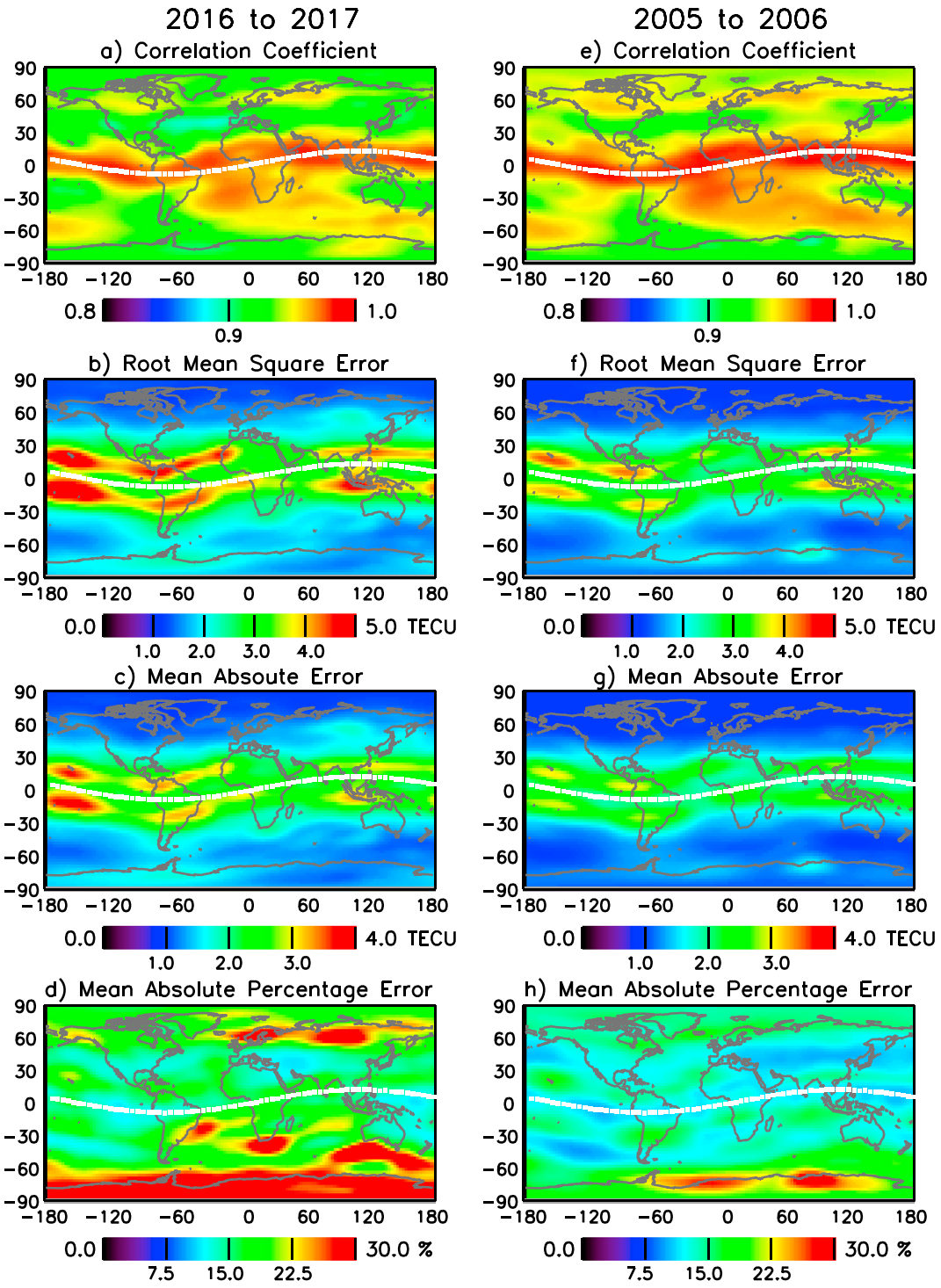

Figure 4. Metrics of the statistical model's regional performance for the 2-year validation period (2016 to 2017), including (a) the correlation of the model and observations, (b) the root-mean-square error (RMSE), (c) the mean absolute error (MAE), and (d) the mean absolute percentage error (MAPE). The metrics (e) correlation coefficient, (f) RMSE, (g) MAE, and (h) MAPE are determined separately for a 2-year period of comparable solar activity (2005 to 2006) in the estimation period. TECU = total electron content unit, 1 TECU = 10^{16} el/m^2.

statistical model to forecast TEC 1 to 10 days into the future, for a range of solar activity conditions, is readily assessed using the IGS database of 2-hourly TEC observations, which extends over more than 18 years. Forecasts of TEC are made using equation (11) at increments of $\Delta t = 1$, 2, 3, 5, 8, and 10 days ahead, at forecast times, t_0, corresponding to the time of each 2-hourly IGS observation, for the duration of the IGS database. Solar EUV irradiance is projected forward to $t_0 + \Delta t$ using an autoregressive representation of the prior 100 days; the *ap* and *Dxt* indices are set to 0 at all times after t_0 (i.e., they are not forecast, autoregressively or otherwise). For comparison with the statistical model forecasts, TEC is also forecast assuming persistence, in which the forecast at time $t_0 + \Delta t$ is equal to the observed value at t_0 (at the same UT), and climatology, for which the value at time $t_0 + \Delta t$ is equal to the average of the observed values (at the same UT) over the prior 10 days. Figure 5 illustrates the approach; shown are the IGS observations and the forecasts made using the statistical model, persistence, and climatology for global TEC and TEC at five different locations (corresponding to those in Figure 3) in two different 10-day intervals. These are two explicit examples of the forecasts that are made at all geographical locations and at every 2-hr interval of the available TEC database. One example (Figure 5, left column) is at the beginning of 2002, during the estimation period when solar activity is near maximum values; the other (Figure 5, left column) is at the beginning of the validation period, when solar activity is more moderate.

3.1. Forecast Performance

The same metrics used in section 2 to assess the statistical model's performance in specifying TEC using actual inputs are used in this section to assess the model's forecast performance using projected inputs. Determined are the RMSE, MAE, and MAPE of the IGS TEC observations and the statistical model's forecasts of TEC at time increments $\Delta t = 1$ to $\Delta t = 10$ days ahead. For example, analogous to equation (9), the MAE of n forecasts of TEC at time increment Δt ahead is

$$MAE_{fc}^{\Delta t} = \frac{1}{n}\sum_{k=1}^{n}\left|TEC_{fc_k}^{\Delta t} - TEC_{\mathrm{obs}_k}\right| \tag{12}$$

where $TEC_{fc_k}^{\Delta t}$ is the forecast and TEC_{obs_k} the observed value of TEC at time $t_0 + \Delta t$. For the persistence forecast

$$MAE_{\mathrm{pers}}^{\Delta t} = \frac{1}{n}\sum_{k=1}^{n}\left|TEC_{\mathrm{obs}_{k-\Delta t}} - TEC_{\mathrm{obs}_k}\right| \tag{13}$$

where $TEC_{\mathrm{obs}_{k-\Delta t}}$ is the TEC observation at the time of the forecast (i.e., at t_0). For the climatology forecast

$$MAE_{\mathrm{ciim}}^{\Delta t} = \frac{1}{n}\sum_{k=1}^{n}\left|\overline{TEC_{\mathrm{obs}_{k-\Delta t}}} - TEC_{\mathrm{obs}_k}\right| \tag{14}$$

where $\overline{TEC_{\mathrm{obs}_{k-\Delta t}}}$ is the average of 10 days of TEC observations prior to and including t_0 (at the same UT).

Shown in Figure 6 are averages over the globe of the MAEs, $MAE_{fc}^{\Delta t}$, of TEC forecasts at $\Delta t = 1$ to $\Delta t = 10$ days (black solid lines) and, for comparison, of global TEC forecasts (black dashed lines) made using the statistical model. Also shown are $MAE_{\mathrm{pers}}^{\Delta t}$ for the persistence forecasts (magenta lines) and $MAE_{\mathrm{clim}}^{\Delta t}$ for the climatology forecasts (blue lines). The $MAE^{\Delta t}$ in Figure 6a (left column) are determined using all 2-hourly forecasts and observations for all months of the 17 years from 1999 to 2015. The $MAE^{\Delta t}$ in Figures 6b and 6c (left column) are determined for all months during 2 years at high and moderate-to-low solar activity in the estimation period, and the $MAE^{\Delta t}$ in Figure 6d are for the 2-year validation period. Table 2 provides numerical values of the $RMSE^{\Delta t}$, $MAE^{\Delta t}$, and $MAPE^{\Delta t}$ performance metrics averaged over the globe of the model's TEC forecasts at $\Delta t = 3$, 5, and 8 days head.

The $MAE^{\Delta t}$ are also evaluated separately for the months of April (Figure 6, middle column) and July (Figure 6, right column). The motivation for assessing the model's performance in individual months (as well as at different levels of solar activity) is that TEC exhibits significant seasonal variability, which the statistical model represents by oscillations at four periods (equation (5)). Global TEC values peak in March–April and October–November, as a result of the SAO, and they are lowest in July, when the AO depresses levels relative to December (Lean, Meier, et al., 2011). The $MAE^{\Delta t}$ shown in Figure 6 (middle and right

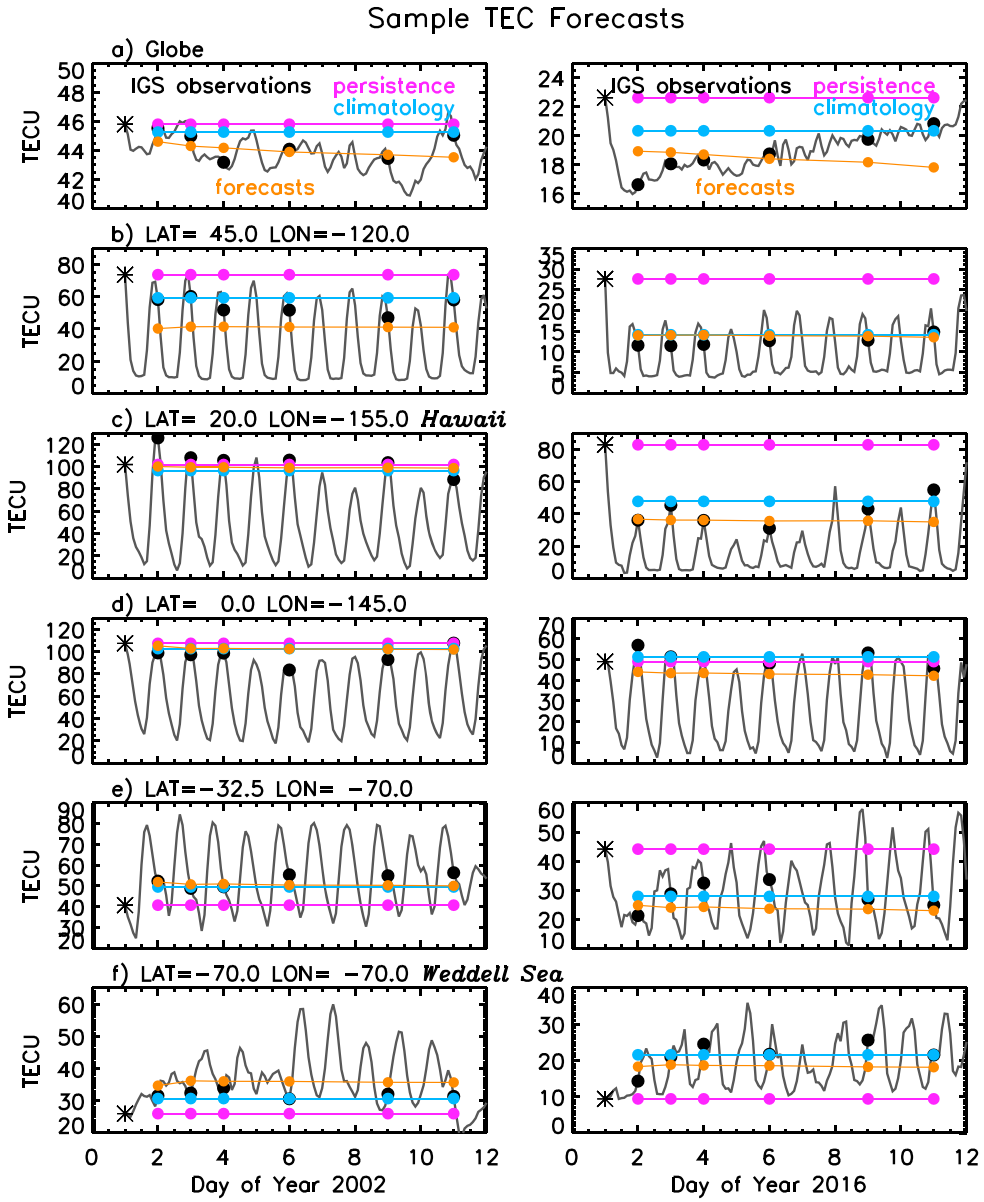

Figure 5. Forecasts of (a) global TEC and (b, c, d, e, and f) forecasts of TEC at individual geographical locations (specifically, those in Figure 3) made at the time indicated by the asterisks, using the statistical model (orange filled circles), persistence (magenta filled circles), and climatology (blue filled circles) compared with the corresponding IGS observations (black filled circles) during two 10-day intervals beginning in January 2002 (on the left column) and January 2016 (on the right column). The solid black lines are the 2-hourly IGS TEC observations. TEC = total electron content; TECU = TEC unit, 1 TECU = 10^{16} el/m^2; IGS = International Global Navigation Satellite Systems Service.

columns) illustrate that the model's performance is indeed seasonally dependent. For the entire period 1999–2015 (Figure 6a) as well as for each of the three different epochs corresponding to high solar activity (Figure 6b), moderate-to-low solar activity (Figure 6c), and the validation period (Figure 6d), the $MAE^{\Delta t}$ are larger in April (middle column, when global TEC maximizes) than in July (right column, when global TEC minimizes). Table 2 includes numerical values of the $RMSE_{fc}^{\Delta t}$, $MAE_{fc}^{\Delta t}$, and $MAPE_{fc}^{\Delta t}$, performance metrics for the statistical model's TEC forecasts in April and July.

As the forecast increment increases from $\Delta t = 1$ to $\Delta t = 10$ days, the $MAE_{fc}^{\Delta t}$ of the statistical model's TEC forecast (determined over the 17 years from 1999 to 2015, Figure 6a) increases from 2.5 to 3.2 TECU. The

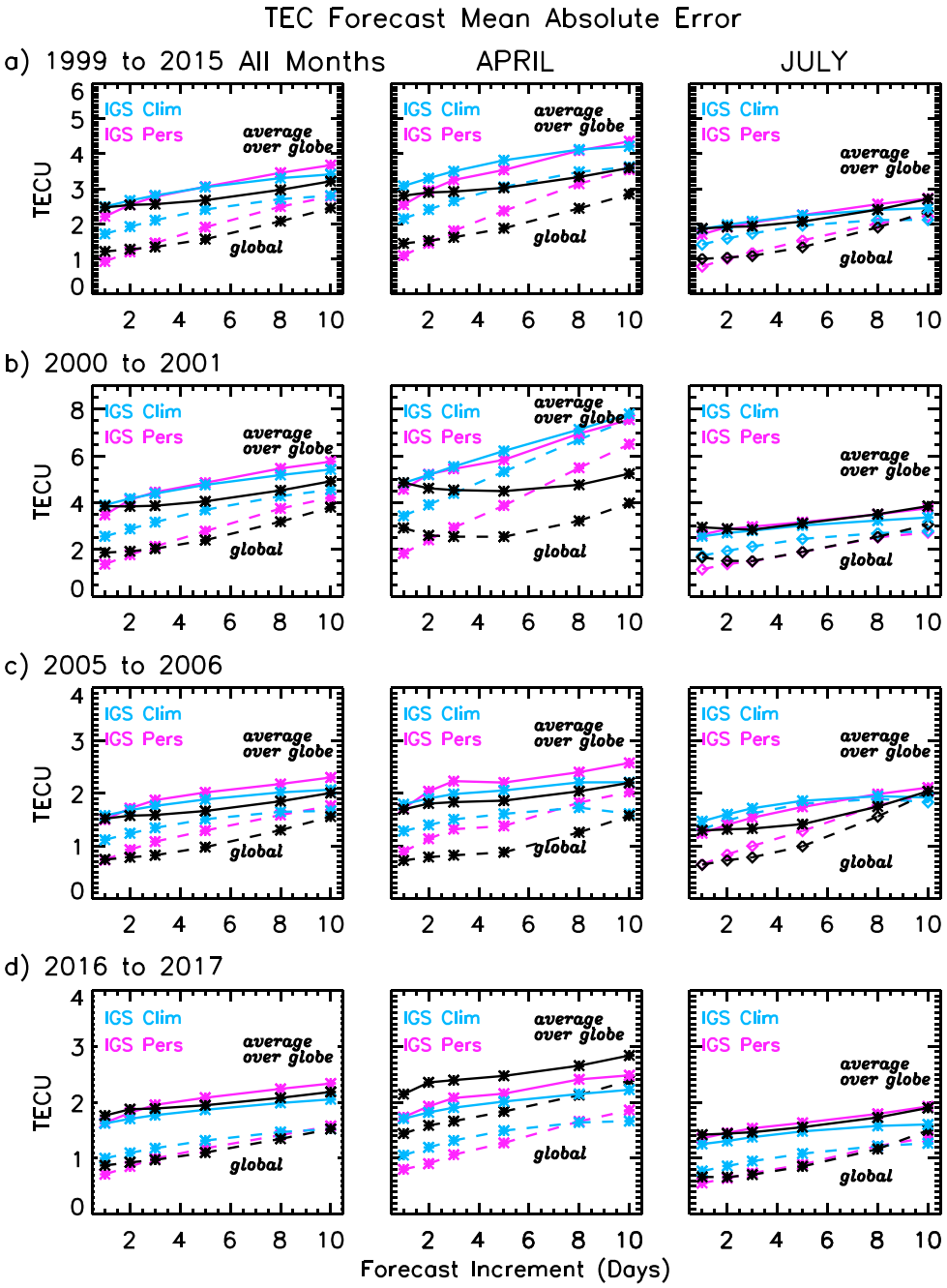

Figure 6. Compared are the mean absolute error of IGS observations and forecasts of TEC at $\Delta t = 1$ to 10 days made using the statistical model ($MAE_{fc}^{\Delta t}$, black), persistence ($MAE_{pers}^{\Delta t}$, magenta), and climatology ($MAE_{clim}^{\Delta t}$, blue) evaluated using 2-hourly values for all months (left column), in April (middle column), and in July (right column) during (a) 1999 to 2015, (b) 2000 to 2001, (c) 2005 to 2006, and (d) 2016 to 2017. The solid lines are the $MAE^{\Delta t}$ of the TEC forecasts averaged over all geographical locations on the globe, and the dashed lines are for the global TEC forecasts. The averages over the globe are numerical averages of the metrics of the performance of the regional statistical model constructed using equation (3) at each of the model's 72 × 71 longitude-latitude grid points. The global TEC metrics pertain to the performance of a separate statistical model of global TEC. IGS = International Global Navigation Satellite Systems Service; TEC = total electron content; TECU = TEC unit, 1 TECU = 10^{16} el/m^2.

$MAE_{\text{pers}}^{\Delta t}$ for the corresponding persistence forecast increases from 2.2 to 3.7 TECU and the $MAE_{\text{clim}}^{\Delta t}$ for the climatology forecast increases from 2.5 to 3.4 TECU. Thus, the errors in the statistical model's forecasts are smaller than the errors in the forecasts made using persistence at Δt = 3, 5, 8, and 10 days, comparable at

Table 2
Metrics of the Performance of the Statistical Model Forecasts of Regional TEC at Time Increments Δt = 3, 5, and 8 Days Ahead, Averaged Over the Globe, at Different Levels of Solar Activity, Estimated Using All 2-Hourly Values on All Days of the Specified Time Intervals and Months

Parameter	1999–2015 Model estimation period Δt = 3, 5, 8	2000–2001 High solar activity Δt = 3, 5, 8	2005–2006 Similar solar activity as model validation Δt = 3, 5, 8	2008–2009 Low solar activity Δt = 3, 5, 8	2016–2017 Model validation period Δt = 3, 5, 8
Root-mean-square error ($RMSE_{fc}^{\Delta t}$, TECU)					
All months	3.8, 4.0, 4.4	5.3, 5.6, 6.2	2.2, 2.3, 2.6	1.3, 1.4, 1.5	2.6, 2.7, 2.8
April	4.2, 4,4, 2,8	6.0, 5.9, 6.2	2.5, 2.5, 2.7	1.4, 1,4, 1,5	3.1, 3.2, 3.5
July	2.8, 3.0, 3.5	3.9, 4.4, 4.8	1.8, 1.9, 2.4	0.9, 0.9, 1.0	2.0, 2.1, 2.3
Mean absolute error ($MAE_{fc}^{\Delta t}$, TECU)					
All months	2.6, 2.7, 3.0	3.9, 4.1, 4.5	1.6, 1.7, 1.9	1.0, 1.0, 1.1	1.9, 2.0, 2.1
April	2.9, 3.0, 3.3	4.5, 4.5, 4.8	1.8, 1.9, 2.0	1.1, 1.1, 1.1	2.4, 2.5, 2.7
July	1.9, 2.1, 2.4	2.9, 3.1, 3.5	1.3, 1.4, 1.8	0.7, 0.7, 0.8	1.5, 1.6, 1.7
Mean absolute percentage error ($MAPE_{fc}^{\Delta t}$, %)					
All months	18, 18, 20	15, 15, 16	17, 17, 19	14, 14, 15	23, 24, 25
April	19, 20, 22	16, 17, 19	17, 18, 19	14, 15, 16	30, 31, 33
July	19, 19, 22	15, 16, 17	17, 17, 21	13, 13, 14	24, 25, 26

Note. TECU = total electron content unit, 1 TECU = 10^{16} el/m^2.

$\Delta t = 2$ days and larger at $\Delta t = 1$ day. Relative to forecasts made using climatology, the errors in the statistical model's forecasts are smaller at $\Delta t = 2$, 3, 5, 8, and 10 days and comparable at $\Delta t = 1$ day.

For all forecasts, whether made using the statistical model, persistence, or climatology, the averages of the $MAE^{\Delta t}$over the globe (solid lines in Figure 6) are, as expected, systematically larger (by about a factor of 2) than the direct forecasts of global TEC (dashed lines in Figure 6). This is because the statistical model of globally integrated TEC variability, which has minimal diurnal variation and muted seasonal variation, is more robust than the model at individual locations. As well, the $MAE^{\Delta t}$ of all the forecasts are larger when solar activity is higher and smaller during solar minimum. For example, as the forecast increment increases from $\Delta t = 1$ to $\Delta t = 10$ days, the $MAE_{fc}^{\Delta t}$ of the statistical model's forecast in the 2-year period of high solar activity (2000 to 2001, Figure 6) increases from 3.9 to 4.9 TECU, during moderate-to-low solar activity (Figure 6c) from 1.5 to 2 TECU and during solar minimum from 0.95 to 1.1 TECU.

Also, independent of the forecast technique (whether using the statistical model, persistence, or climatology), and of solar activity as well, the $MAE^{\Delta t}$ in Figure 6 (and the $MAE^{\Delta t}$and $RMSE^{\Delta t}$ in Table 2) are larger in April (when the SAO peaks in global TEC) and smaller in July (when global TEC is at its minimum value for the year). For example, the $MAE_{fc}^{\Delta t}$ of the statistical model's TEC forecasts at Δt= 3, 5, and 8 days are 2.6, 2.7, and 3 TECU, respectively, when determined using all months from 1999 to 2015, Figure 6a) but increase to 2.9, 3, and 3.3 TECU in April and decrease to 1.9, 2.1, and 2.4 TECU in July.

The $MAE^{\Delta t}$ of the forecasts have a distinct regional pattern that manifests irrespective of the value of the forecast time increment, Δt, or of the forecasting approach. Shown in Figure 7 are the regional distributions of $MAE_{fc}^{\Delta t}$ for the statistical model's Δt = 3- and Δt = 8-day forecasts (Figures 7a and 7d), $MAE_{\text{pers}}^{\Delta t}$ for the corresponding forecasts using persistence (Figures 7b and 7e), and $MAE_{\text{clim}}^{\Delta t}$ for the forecasts using climatology (Figure 7c and 7f). The $MAE^{\Delta t}$ are uniformly larger in the low-latitude EIA region, where TEC itself maximizes, and where the MAE and RMSE metrics of the statistical model performance are also largest (Figures 2 and 4). In some EIA regions, the $MAE_{fc}^{\Delta t}$ of the TEC forecasts $\Delta t = 3$ days ahead reach 5 TECU and the $MAE_{fc}^{\Delta t}$ of the TEC forecasts $\Delta t = 8$ days ahead reach 6 TECU. But less regions in the EIA have these higher values in the statistical model forecasts than in the persistence and climatology forecasts (compare Figure 7a with Figures 7b and 7c for the 3-day forecasts, and Figure 7d with Figures 7e and 7f for the 8-

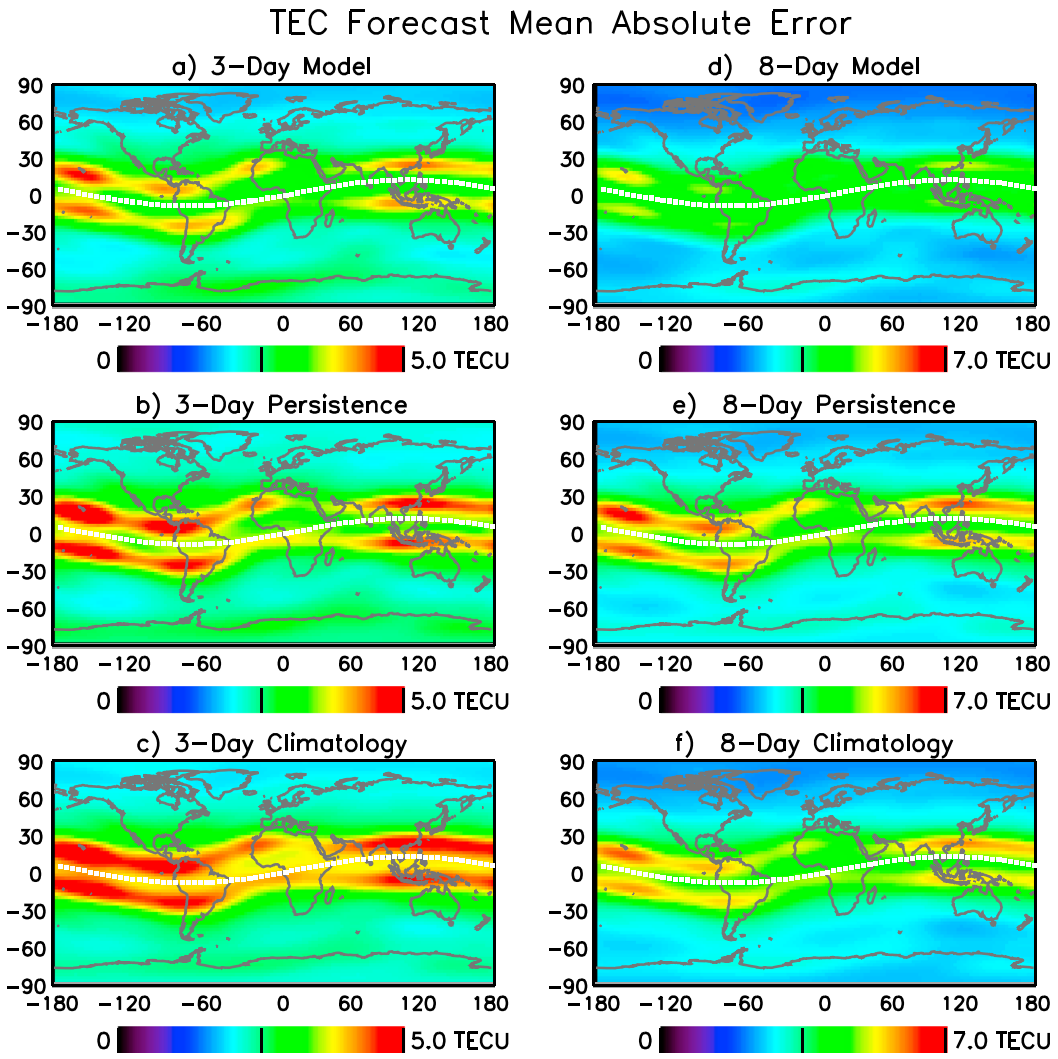

Figure 7. The regional distributions of the mean absolute error of forecasts of TEC made at 2-hr intervals for all months from 1999 to 2015 at Δt = 3 days using (a) the statistical model, (b) persistence, and (c) climatology, and at Δt = 8 days using (d) the statistical model, (e) persistence, and (f) climatology. The averages of the maps are the values at Δt = 3 and Δt = 8 days in Figure 6a for all months. TEC = total electron content; TECU = TEC unit, 1 TECU = 10^{16} el/m^2.

day forecasts). As a result the $RMSE^{\Delta t}$ and $MAE^{\Delta t}$ averaged over low latitudes (30°S to 30°N) are smaller for the statistical model forecasts than for the forecasts using persistence or climatology.

Table 3 lists numerical values for the $RMSE_{fc}^{\Delta t}$, $MAE_{fc}^{\Delta t}$, and $MAPE_{fc}^{\Delta t}$ of the statistical model forecasts, the $RMSE_{\text{pers}}^{\Delta t}$, $MAE_{\text{pers}}^{\Delta t}$, and $MAPE_{\text{pers}}^{\Delta t}$ for the forecasts using persistence and the $RMSE_{\text{clim}}^{\Delta t}$, $MAE_{\text{clim}}^{\Delta t}$, and $MAPE_{\text{clim}}^{\Delta t}$ for the forecasts using climatology, averaged over the globe and separately over low (30°S to 30°N) and middle (60°S to 30°S, 30°N to 60°N) latitudes, determined for the estimation period. Averaged over 30°S to 30°N, forecasts at Δt = 3 days made using the statistical model have $MAE_{fc}^{\Delta t}$ = 3.3 TECU compared with $MAE_{\text{pers}}^{\Delta t}$ = 3.6 TECU using persistence and $MAE_{\text{clim}}^{\Delta t}$ = 3.8 TECU using climatology. For forecasts at Δt = 8 days, $MAE_{fc}^{\Delta t}$ = 3.9 TECU for the statistical model, $MAE_{\text{pers}}^{\Delta t}$ = 4.7 TECU for persistence, and $MAE_{\text{clim}}^{\Delta t}$ = 4.5 TECU for climatology. More generally, the numerical values in Table 3 show that according to both the $RMSE^{\Delta t}$ and $MAE^{\Delta t}$ metrics averaged over all latitudes and at low and middle latitudes, the errors of the Δt= 3-, 5-, 8-, and 10-day forecasts using the statistical model are systematically smaller than the forecast errors using persistence and climatology. Only for forecasts at Δt= 1 day do the $RMSE_{fc}^{\Delta t}$ and $MAE_{fc}^{\Delta t}$ of the statistical model exceed the $RMSE_{\text{pers}}^{\Delta t}$ and $MAE_{\text{pers}}^{\Delta t}$ for the persistence forecasts.

Table 3
The Root-Mean-Square Error, $RMSE_{fc}^{\Delta t}$, Mean Absolute Error, $MAE_{fc}^{\Delta t}$, and Mean Absolute Percentage Error, $MPAE_{fc}^{\Delta t}$, of TEC Observations and the Statistical Model Forecasts at Time Increments Δt = 1, 3, 5, 8, and 10 Days Ahead, Averaged Over the Globe and at Low (30°S–30°N), Midnorthern (30–60°N) and Midsouthern (30–60°S) Latitudes, Compared With Equivalent Metrics for Forecasts Made Using Persistence $\left(RMSE_{pers}^{\Delta t}, MAE_{pers}^{\Delta t}, MAPE_{pers}^{\Delta t}\right)$ and Climatology $\left(RMSE_{clim}^{\Delta t}, MAE_{clim}^{\Delta t}, MAPE_{clim}^{\Delta t}\right)$ of the Observations, Estimated Using All 2-Hourly Values During the Estimation Period (1999–2015)

	Statistical model	Persistence	Climatology
Parameter	Δt = 1, 3, 5, 8, 10	Δt = 1, 3, 5, 8, 10	Δt = 1, 3, 5, 8, 10
Root-mean-square error (TECU)			
Average over globe	3.7, 3.8, 4.0, 4.4, 4.8	3.5, 4.3, 4.7, 5.2, 5.6	3.8, 4.3, 4.6, 5.0, 5.1
30°S–30°N	4.6, 4.8, 5.0, 5.8, 6.4	4.4, 5.3, 6.0, 6.9, 7.4	5.0, 5.7, 6.2, 6.8, 7.0
30–60°N	3.3, 3.4, 3.6, 3.9, 4.4	3.1, 3.8, 4.1, 4.6, 4.9	3.4, 3.8, 4.1, 4.4, 4.5
30–60°S	3.3, 3.4, 3.6, 3.9, 4.2	3.1, 3.8, 4.2, 4.7, 5.0	3.4, 3.8, 4.1, 4.5, 4.6
Mean absolute error (TECU)			
Average over globe	2.5, 2.6, 2.7, 3.0, 3.2	2.2, 2.8, 3.1, 3.5, 3.7	2.5, 2.8, 3.1, 3.3, 3.4
30°S–30°N	3.2, 3.3, 3.5, 3.9, 4.3	2.9, 3.6, 4.0, 4.7, 5.0	3.4, 3.8, 4.2, 4.5, 4.7
30–60°N	2.2, 2.3, 2.4, 2.6, 2.8	1.9, 2.4, 2.7, 3.0, 3.2	2.2, 2.4, 2.7, 2.9, 2.9
30–60°S	2.2, 2.3, 2.4, 2.6, 2.8	1.9, 2.4, 2.6, 3.0, 3.2	2.2, 2.4, 2.7, 2.9, 3.0
Mean absolute percentage error (%)			
Average over globe	16, 18, 18, 20, 21	14, 17, 19, 20, 22	15, 17, 18, 19, 20
30°S–30°N	13, 13, 14, 15, 17	11, 14, 15, 17, 19	13, 14, 15, 17, 17
30–60°N	14, 15, 16, 17, 18	12, 15, 17, 18, 20	13, 15, 16, 17, 18
30–60°S	16, 17, 18, 20, 21	13, 16, 18, 20, 21	14, 16, 17, 19, 20

Note. TECU = total electron content unit, 1 TECU = 10^{16} el/m^2.

3.2. Forecast Skill Score

To further quantify the statistical model's forecasting capability, skill scores are calculated by comparing performance metrics of the statistical model's TEC forecasts with those for forecasts made using persistence and climatology. For example, the skill scores of the statistical model's $MAE_{fc}^{\Delta t}$ relative to persistence and climatology are (Wilks, 1995), respectively,

$$SSMAE_{\text{pers}}^{\Delta t} = 1 - \frac{MAE_{fc}^{\Delta t}}{MAE_{\text{pers}}^{\Delta t}} \tag{15}$$

$$SSMAE_{\text{clim}}^{\Delta t} = 1 - \frac{MAE_{fc}^{\Delta t}}{MAE_{\text{clim}}^{\Delta t}} \tag{16}$$

where examples of the numerical values of $MAE_{fc}^{\Delta t}$, $MAE_{\text{pers}}^{\Delta t}$, and $MAE_{\text{clim}}^{\Delta t}$ are listed in Table 3. Figure 8 shows the model's $SSMAE^{\Delta t}$skill scores averaged over the globe for TEC forecasts Δt = 1 to 10 days ahead, and also the corresponding $SSRMSE^{\Delta t}$ skill scores, evaluated using $RMSE^{\Delta t}$ (Table 3) in place of $MAE^{\Delta t}$in equations (15) and (16). The skill scores are evaluated using all 2-hr forecasts during the estimation period (Figure 8a), during high solar activity (Figure 8b), moderate-to-low solar activity (Figure 8c), and for the validation period (Figure 8d). As expected from comparisons of the forecast performance metrics in the previous section, in the estimation period (Figures 8a–8c) the skill scores of the statistical model's Δt = 3-, 5-, 8-, and 10-day TEC forecasts systematically exceed persistence and climatology. For example, the average over the globe of the skill score of the statistical model's Δt = 5-day forecast is 12% and 11% relative to persistence and climatology according to the $MAE^{\Delta t}$metrics and 15% and 13% relative to persistence and climatology according to the $RMSE^{\Delta t}$metrics. Only for forecasts at time increment Δt = 1 day is the skill score of the statistical model's forecast negative, indicating that at this shortest time increment errors in the statistical model forecasts during the estimation period averaged over the globe are larger than in the forecasts using persistence. As Figure 8d shows, the skill of forecasts at increments Δt = 3, 5, 8, and 10 days ahead during the 2-year validation period exceeds persistence but not climatology.

The skill scores of the statistical model's TEC forecasts depend on season. At all time increments from Δt = 1 to Δt = 10 days ahead, forecast skill relative to both persistence and climatology is higher in April than in

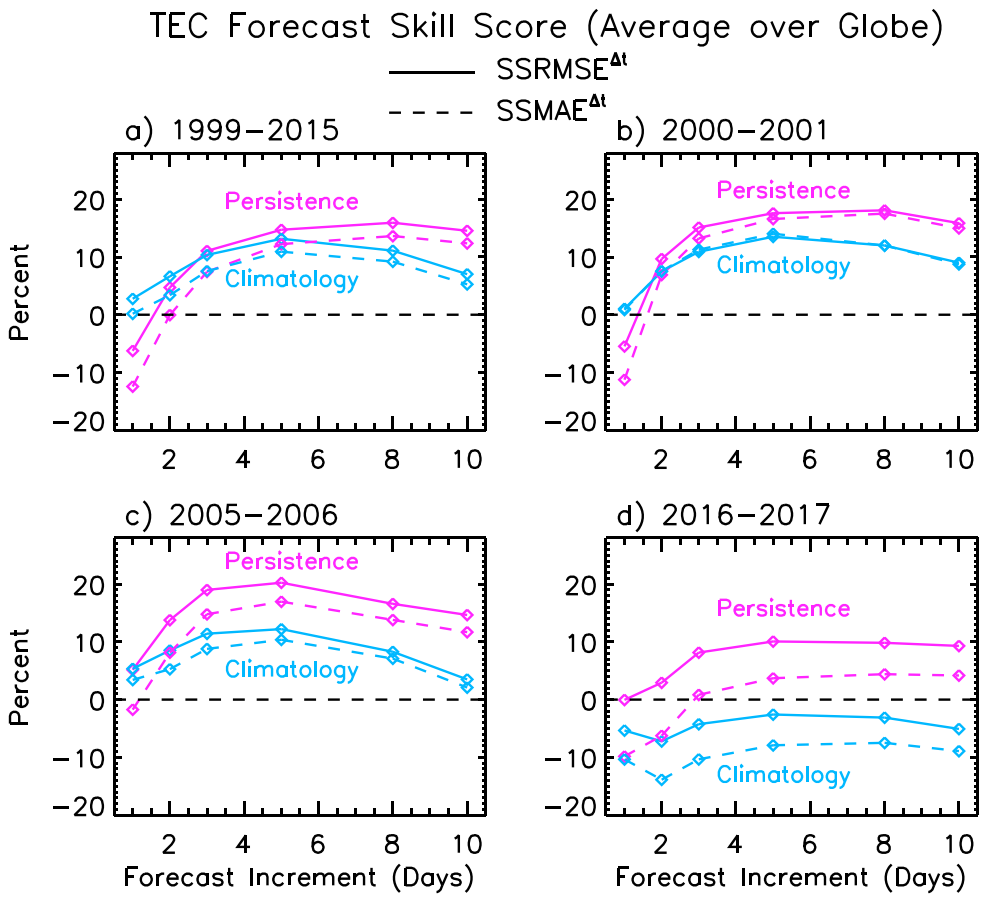

Figure 8. Skill scores averaged over the globe of the statistical model forecasts at $\Delta t = 1$ to 10 days ahead relative to persistence and climatology, estimated using all 2-hr forecasts during (a) 1999 to 2015, (b) 2000–2001, (c) 2005–2006, and (d) 2016–2017. The solid lines are skill scores pertaining to the root-mean-square error of the forecasts, $SSRMSE^{\Delta t}$, and the dashed lines are skill scores pertaining to the absolute mean error of the forecasts, $SSMAE^{\Delta t}$.

July. Figure 9 shows the seasonal dependence of the statistical model's skill scores relative to both persistence and climatology, based on both the $RMSE^{\Delta t}$ and $MAE^{\Delta t}$ performance metrics (determined using the forecasts in the estimation period). For the $\Delta t = 5$ day forecasts in Figure 9d, for example, the statistical model forecasts averaged over the globe exceed persistence by ~15% and climatology by ~20% in April but only by ~5% in July.

As well as depending on season, the skill scores of the statistical model's TEC forecasts depend on geographical location. Figure 10 shows the regional distributions of the statistical model's 3- and 8-day TEC forecast skill scores relative to persistence and climatology in April (Figures 10a, 10b, 10e, and 10f) and July (Figures 10c, 10d, 10g, and 10h). In April, the statistical model's forecast skill scores are positive over most of the globe, in the range 10% to 40% relative to persistence and climatology, the exception being over a modest area at high southern latitudes in the vicinity of the Weddell Sea where the skill score is as much as 40% negative. In July, however, the statistical model's forecast skill scores are overall lower, exceeding persistence and climatology only in the Northern Hemisphere and at low Southern Hemisphere latitudes, and only by 10% or less, and underperforming relative to both persistence ad climatology over most high southern latitudes, especially in an expanded area around the Weddell Sea.

4. Discussion

4.1. Model Forecast Skill

The statistical model of TEC variability, per se, is simple, straightforward, and concise; it specifies TEC without the need for real-time observations, using instead parameterizations of TEC variability associated with

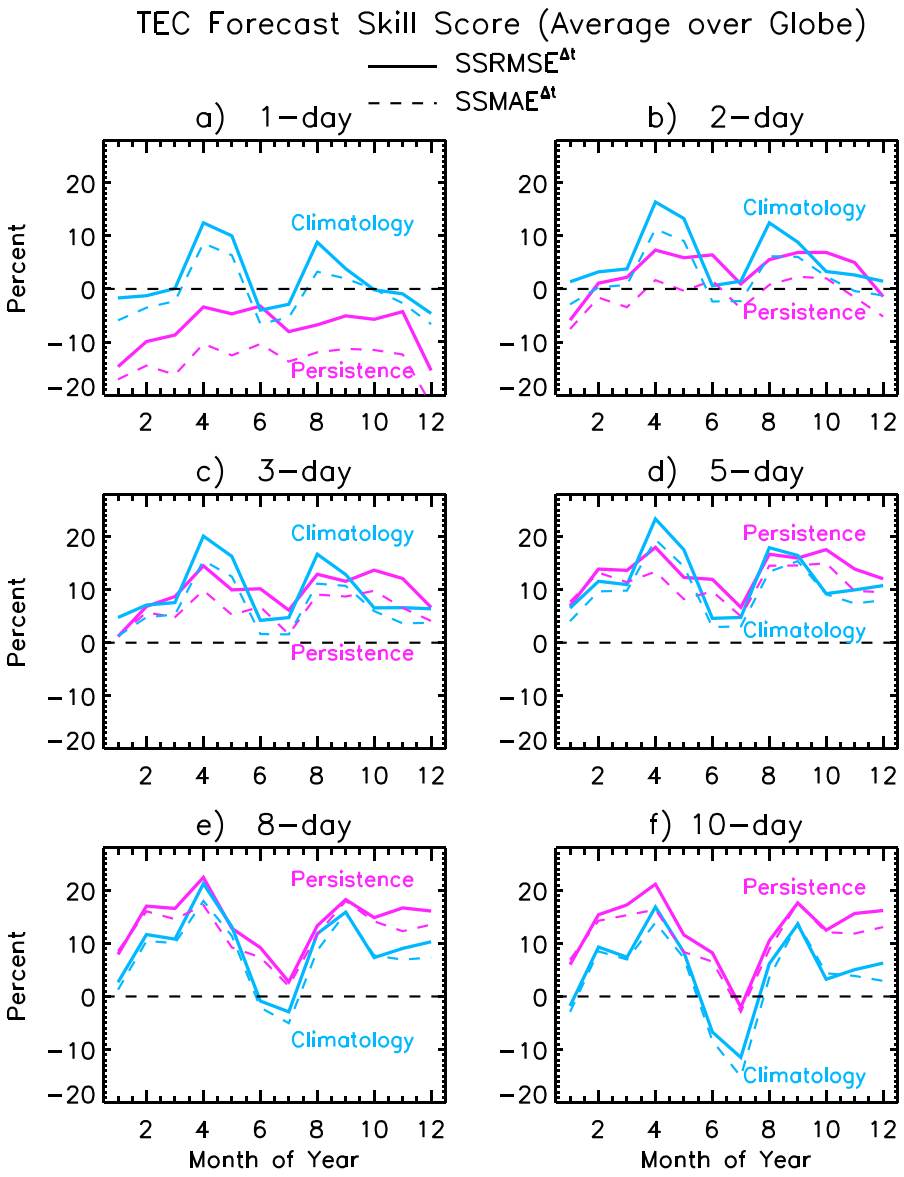

Figure 9. The skill scores averaged over the globe of the statistical model forecasts relative to persistence and climatology for different months of the year for forecast time increments (a) $\Delta t = 1$, (b) $\Delta t = 2$, (c) $\Delta t = 3$, (d) $\Delta t = 5$ days, (e) $\Delta t = 8$, and (f) $\Delta t = 10$ days ahead. The skill scores are evaluated using all forecast made during each month between 1999 and 2015. The solid lines are the skill scores pertaining to the root-mean-square error of the forecasts, $SSRMSE^{\Delta t}$, and the dashed lines are skill scores pertaining to the absolute mean error of the forecasts, $SSMAE^{\Delta t}$.

solar and geomagnetic activity and seasonal and diurnal oscillations in past observations. The fidelity of the estimates of future solar EUV irradiance and geomagnetic activity that are input to the model are key determinants of the model's ability to forecast TEC. Significant autocorrelation in the EUV irradiance time series enables autoregressive projections of future values; the autocorrelation is ~1 at a lag of 1 day, 0.97 at a lag of 5 days, and 0.94 at a lag of 8 days. Using autoregressive forecasts of daily EUV irradiance based on known values of the prior 100 days, the statistical model forecasts TEC at $\Delta t = 3$, 5, and 8 days for t_0 every 2 hr from 1999 to 2015 with $RMSE_{fc}^{\Delta t} = 3.8$, 4.0, and 4.4 TECU and $MAE_{fc}^{\Delta t} = 2.6$, 2.7, and 3 TECU averaged over the globe (Table 2); the increasing error of the forecasts at longer forecast time increments mimics the decrease in the autocorrelation of the EUV irradiance at larger lags. The model's geomagnetic inputs are not forecast because autocorrelation in the geomagnetic activity time series is minimal; it is 0.28 at a lag of 1 day and <0.1 at lags of 5 and 8 days.

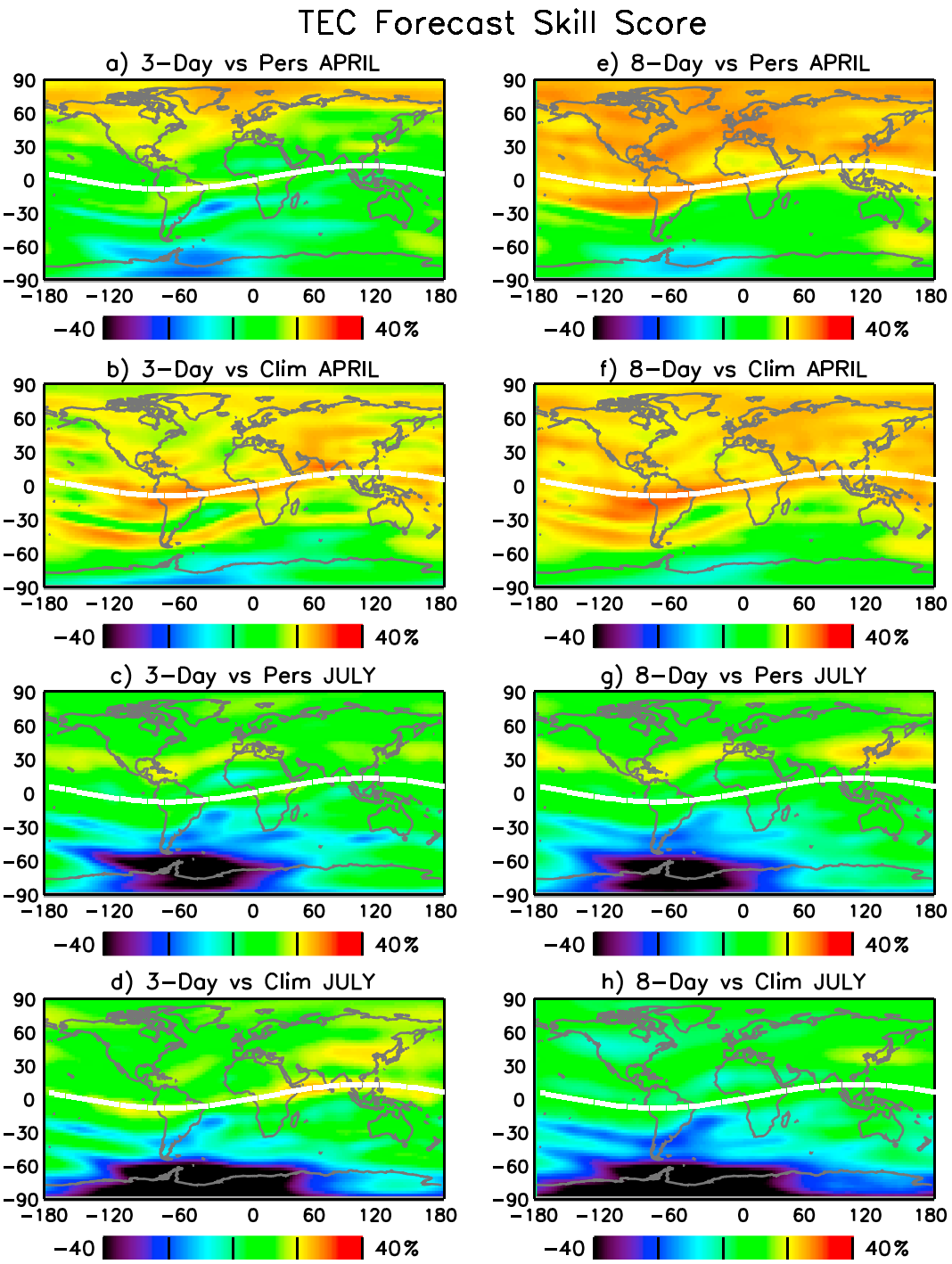

Figure 10. The regional distributions of the skill scores of the statistical model forecasts at $\Delta t = 3$ days relative to persistence, $SSMAE^{\Delta t}_{pers}$, in (a) April and (c) July and relative to climatology, $SSMAE^{\Delta t}_{clim}$, in (b) April and (d) July. The regional distributions of the skill scores of the statistical model forecasts at $\Delta t = 8$ days relative to persistence, $SSMAE^{\Delta t}_{pers}$, in (e) April and (g) July and relative to climatology, $SSMAE^{\Delta t}_{clim}$, in (f) April and (h) July. The skill scores are for TEC forecasts made at 2-hr intervals throughout 1999 to 2015 in the specified month. The averages of the maps are shown as the values for April (month 4) and July (month 7) for the forecasts at time increment $\Delta t = 3$ in Figure 9c and at $\Delta t = 8$ in Figure 9e. TEC = total electron content.

The skill scores of the statistical model's TEC forecasts at time increments $\Delta t = 3$, 5, 8, and 10 days ahead for forecasts made at 2-hourly intervals from 1999 to 2015 are positive relative to persistence and climatology. This may be in part because changing solar EUV irradiance alters TEC on these times scales, so autoregressive forecasts of future EUV irradiance improve the TEC forecasts. Larger-than-average forecast errors in regions within the EIA, and also at high southern latitudes surrounding the Weddell Sea, may be the result of meteorological influences from the lower atmosphere that the statistical model does not include. That similar regionally inhomogeneous errors are present in the statistical model, persistence and climatological forecasts suggests that the larger uncertainty (in absolute TECU) of forecasts in these regions may be because TEC is inherently more variable, whether from additional influences that the model does not include or from observational limitations of the IGS TEC database and hence more difficult to forecast at these locations. At high southern latitudes, in particular, the errors in the forecasts made using persistence and climatology are smaller than in the statistical model forecasts. One explanation is that the larger uncertainties in GPS-derived TEC observations over the southern ocean and at high southern latitudes (due to the lack of GPS ground receivers) preclude the statistical model parameterizations from properly capturing TEC variability in these regions; consistent with this, the statistical model specifications in the estimation period themselves have largest errors at high southern latitudes.

The statistical model performs less well in forecasting TEC during 2016 and 2017, the validation period, than in the estimation period from 2005 to 2006, for which solar and geomagnetic activity are approximately comparable. One possible reason is that the model itself does not perform as well in specifying TEC during the validation period as in the estimation period, from which the model was constructed. If so, the errors in the statistical model forecasts determined for the estimation period may underestimate the actual errors (by 10% to 40%, depending on season) when using the statistical model in epochs beyond the estimation period. A second reason is that while solar and geophysical conditions in the validation period are comparable to those in the estimation period from 2005 to 2006, they are not truly equivalent.

Rigorous validation of the model's forecast skill ultimately requires many more years of observations with greater reliability over the entire globe and over a much wider range of solar activity. Figure 4d shows that the largest MAPE of the observations and model in the validation period occur at high southern latitudes, where TEC itself is lowest, the IGS observations least certain, and the model uncertainties therefore largest. In global TEC, the largest differences between the model and observations in the validation period occur in March and April 2016 when the observed global TEC (18.98 TECU) is 6% less than the modeled TEC (20.22 TECU); the MAPE of the forecasts in the validation period (Table 2) are correspondingly highest in April. But whether the source of the differences lies with the model or the IGS observations is indeterminant; the differences are within the likely uncertainty of the IGS TEC observations.

4.2. Forecasts on Time Scales of Months and Years

Forecasts of TEC are possible on time scales longer than 1 to 10 days ahead, given forecasts of the statistical model's solar EUV irradiance and geomagnetic inputs. However, the autoregressive projections of the solar EUV irradiance used for forecasting TEC at $\Delta t = 1$ to $\Delta t = 10$ days ahead become less useful on these longer time scales; the autocorrelation of EUV irradiance at 90 days, for example, is 0.88, whereas at 5 days it is 0.97. This reflects the physical solar processes by which solar activity alters EUV irradiance. The lifetimes of bright active regions whose presence in the solar atmosphere increases EUV irradiance are typically weeks to a month. Furthermore, the Sun's rotation means that an active region that emerges on the east limb of the solar disc is present on the solar hemisphere projected to Earth for at most 13 days, with maximum effect after 7 days when it is at the central meridian (i.e., projected directly to Earth). This is consistent with the average skill of the statistical model forecasts relative to both persistence and climatology being highest at 5 to 8 days and decreasing thereafter. However, epochs in which large, long-lived active regions return to the hemisphere projected to Earth (typically during periods of high solar activity) may afford forecast skill at 27 days; the autocorrelation of EUV irradiance increases from a local minimum of 0.91 at 14 days to a local maximum of 0.96 at 27 days.

The National Oceanic and Atmospheric Administration SWPC issues projections of solar activity in future months and years. A relationship between monthly sunspot numbers and monthly EUV irradiance enables estimates of the EUV irradiance inputs to the statistical model of TEC variability using the sunspot numbers that SWPC forecasts. Shown in Figure 11 are statistical model forecasts (green) of global TEC made using

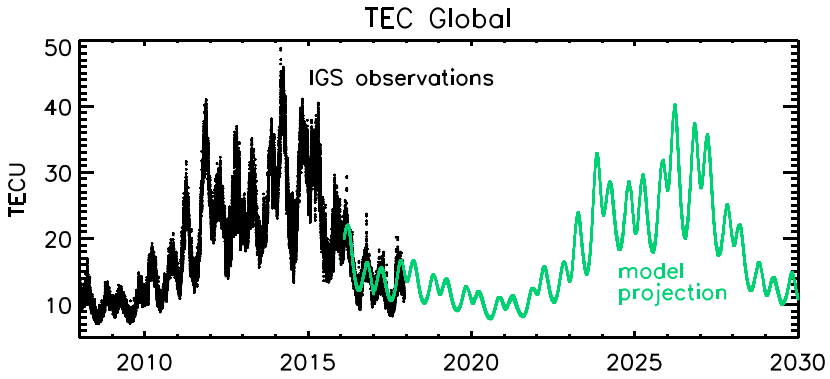

Figure 11. The time series of global TEC from Figure 1 is extended to future years 2019 to 2030 by inputting to the statistical model estimates of monthly total EUV irradiance obtained from a parameterization of total EUV irradiance (Figure 1) and sunspot numbers. The TEC values projected for 2017 to 2019 use the Space Weather Prediction Center forecasts of monthly sunspot numbers for those years. TEC projections from 2020 to 2030 assume that solar activity in cycle 25 will be similar to that in cycle 24. TEC = total electron content; EUV = extreme ultraviolet; IGS = International Global Navigation Satellite Systems Service; TECU = TEC unit, 1 TECU = 10^{16} el/m^2.

solar EUV irradiance inputs derived from the SWPC forecasts of the monthly sunspot number index of solar activity for 2017 to 2019. The overlap of the TEC forecasts with the actual observations (black) indicates overall good agreement.

The projections shown In Figure 11 of global TEC from 2020 to 2030 utilize the emerging expectation that upcoming solar activity in cycle 25 will be comparable to that in cycle 24. This is based on recent observations that the polar fields during the current solar minimum appear very similar in strength to those in the prior solar minimum. Since uncertainty in long-range—monthly to yearly—TEC forecasts derives directly from uncertainty in the solar activity forecasts themselves (which exceed 50%), the skill of the statistical model's long-range forecasts may be expected to increase with advances in forecasting future solar activity. Validation of the TEC projections in Figure 11 await future observations.

4.3. Statistical Model Representation of Geomagnetic Activity

In the statistical model's forecasts of TEC at $\Delta t = 1$ to $\Delta t = 10$ days ahead the indices *ap* and *Dxt* are set to 0 at times beyond the time, t_0, at which the forecast is made. This is because the minimal autocorrelation of the geomagnetic activity indices precludes their autoregressive forecasting. Current state-of-the-art techniques for forecasting geomagnetic activity utilize independent observations of coronal mass ejections and their perturbation of the ambient solar wind speed and density (e.g., Tsagouri et al., 2018). The SWPC does provide 3-day forecasts of *ap*; whether use of these forecasts improves the statistical model's TEC forecasts requires further analysis analogous to that described here using the EUV irradiance forecasts, if independent *ap* and *Dxt* forecasts are available over the past two decades.

A prerequisite for a model, whether empirical or physical, to forecast the ionosphere's response to geomagnetic activity is that the model properly specify the real-time response. A community challenge recently sought to quantify the capability of a suite of models to reproduce the TEC variations observed during an ionospheric storm on 14–15 December 2006, using known (not forecast) geomagnetic activity. Of the eight different models participating in the challenge (Shim et al., 2017, Table 1) one is an empirical model (IRI), two are physics-based ionospheric models (USU-IFM and SAMI3), four are physics-based coupled ionosphere-thermosphere models (TIE-GCM, CTIPE, UAM, and GITM), and one is a physics-based data assimilation model (USU-GAIM), each with different longitude-latitude grid resolution and height of the upper boundary for calculating TEC. One metric of model performance that the challenge adopted is the RMSE of the change in TEC at the peak of the positive phase of the storm from prestorm levels, averaged over the globe and over low to middle latitudes (in this case defined as 50°S to 50°N). Among the seven nonassimilative models, this RMSE ranges from 6.8 to 10.3 TECU when averaged over the globe and from 7.2 to 11.3 TECU when averaged over low to middle latitudes (Shim et al., 2017, Table 2b, Global RMSE column).

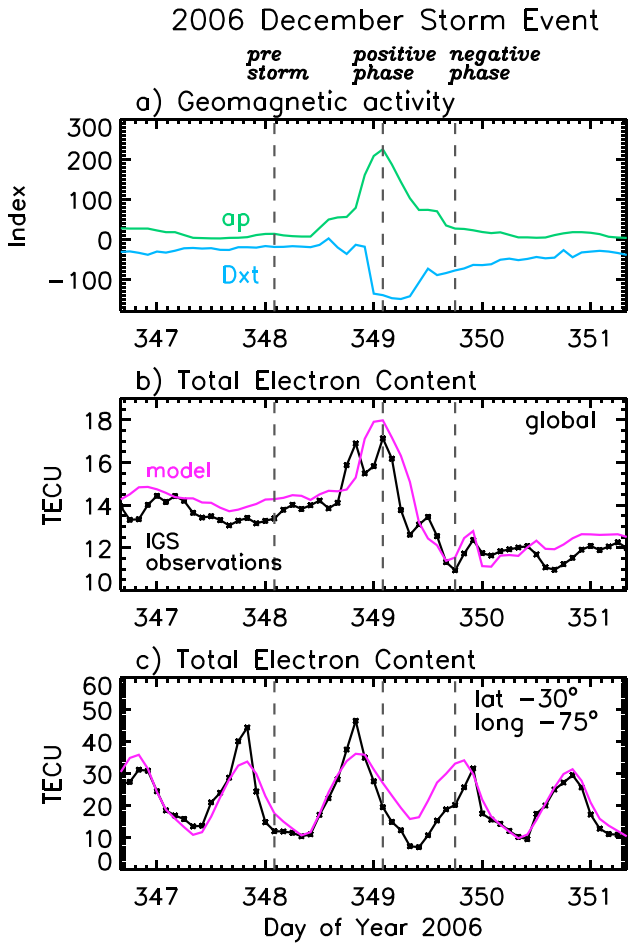

Figure 12. (a) The *ap* and *Dxt* geomagnetic indices during the December 2006 storm event, which was the focus of a community "challenge" designed to quantify extant model capability for specifying TEC changes during, primarily, the positive phase of an ionospheric storm. Shown during the corresponding time are the International Global Navigation Satellite Systems Service observations and the statistical model determinations of (b) global TEC and (c) regional TEC at 30°S, 75°W. Like the other simulations in the community challenge, the statistical model calculations utilized real-time solar activity and geomagnetic inputs, not actual forecasts of these inputs. TEC = total electron content; TECU = TEC unit, 1 TECU = 10^{16} el/m^2.

Figure 12a shows the variations of the *ap* and *Dxt* indices during the December 2006 storm and concurrent variations in TEC according to both the IGS observations and specified by the statistical model globally (Figure 12b) and at a specific site (30°S, 75°W, Figure 12c). Note that the time series of both *ap* and *Dxt* in Figure 12a, and used for input to the statistical model to estimate the TEC changes in Figures 12b and 12c, are (as in Shim et al., 2017) the actual observed values, not forecast values. While an overall increase is evident in global TEC during the storm, approximately aligned with the peak in geomagnetic activity, the much larger local TEC diurnal cycle at 30°S, 75°W obscures evidence for the accompanying regional TEC change. For this reason, to quantify regional TEC changes at the peak of the storm from pre storm levels, the challenge compared simulated TEC values at the peak of the storm's positive phase with prestorm levels 1 day prior. The dashed lines in Figure 12 identify these specific times, as well as the time of the maximum negative phase of the storm.

The comparisons in Figure 13 of the observations and statistical model's specification of regional TEC 1 day prior to the storm (Figure 13a), during the storm's peak positive phase (Figure 13b) and during the peak of the negative phase (Figure 13c), serve to quantify the model's performance during this particular geomagnetic storm, for comparison with the model simulations in the community challenge. The difference of the IGS observations and the statistical model specification in Figure 13b (the positive phase "IGS minus Model" image) minus the difference of the IGS observations and statistical model specification in Figure 13a (the prestorm IGS minus Model image) is equivalent to what the community challenge denotes as the change in TEC at the peak of the positive phase of the storm from prestorm levels. The corresponding metrics for the statistical model are RMSE = 6.8 TECU for the differences averaged over the globe and RMSE = 8.1 TECU for the differences averaged over low to middle latitudes (50°S to 50°N).

The metrics of the statistical model's performance in specifying TEC changes during the December 2006 geomagnetic storm are comparable to those of the better-performing, nonassimilative models in the community challenge. This is consistent with the finding of the challenge that the performance of the IRI model, also an empirical model constructed from observations, in specifying TEC changes during this storm exceeds that of most nonassimilative physical models of the ionosphere. Shim et al. (2017) caveat this finding by noting that while an empirical model such as IRI may perform comparably to physics-based models in terms of some metrics "they represent the average ionospheric conditions rather than storm time perturbations." Perhaps more importantly, the robust quantification of any model's representation of storm-induced TEC changes requires metrics assembled for multiple storms, not just a single event; this is in progress using the statistical model and IGS observations for dozens of storms since 1998, analogous to the metrics for the 14–15 December 2006 storm.

5. Summary

Forecasts are made of regional and global ionospheric TEC at time increments of $\Delta t = 1, 2, 3, 5, 8$, and 10 days ahead in 2-hourly steps for the duration of the IGS TEC observations (1999 to 2017). The forecasts use a statistical model constructed from IGS observations from 1998 to 2015. In contrast to current operational capabilities that assimilate extensive observations to specify near-real-time TEC, and forecast TEC up to 24 hr

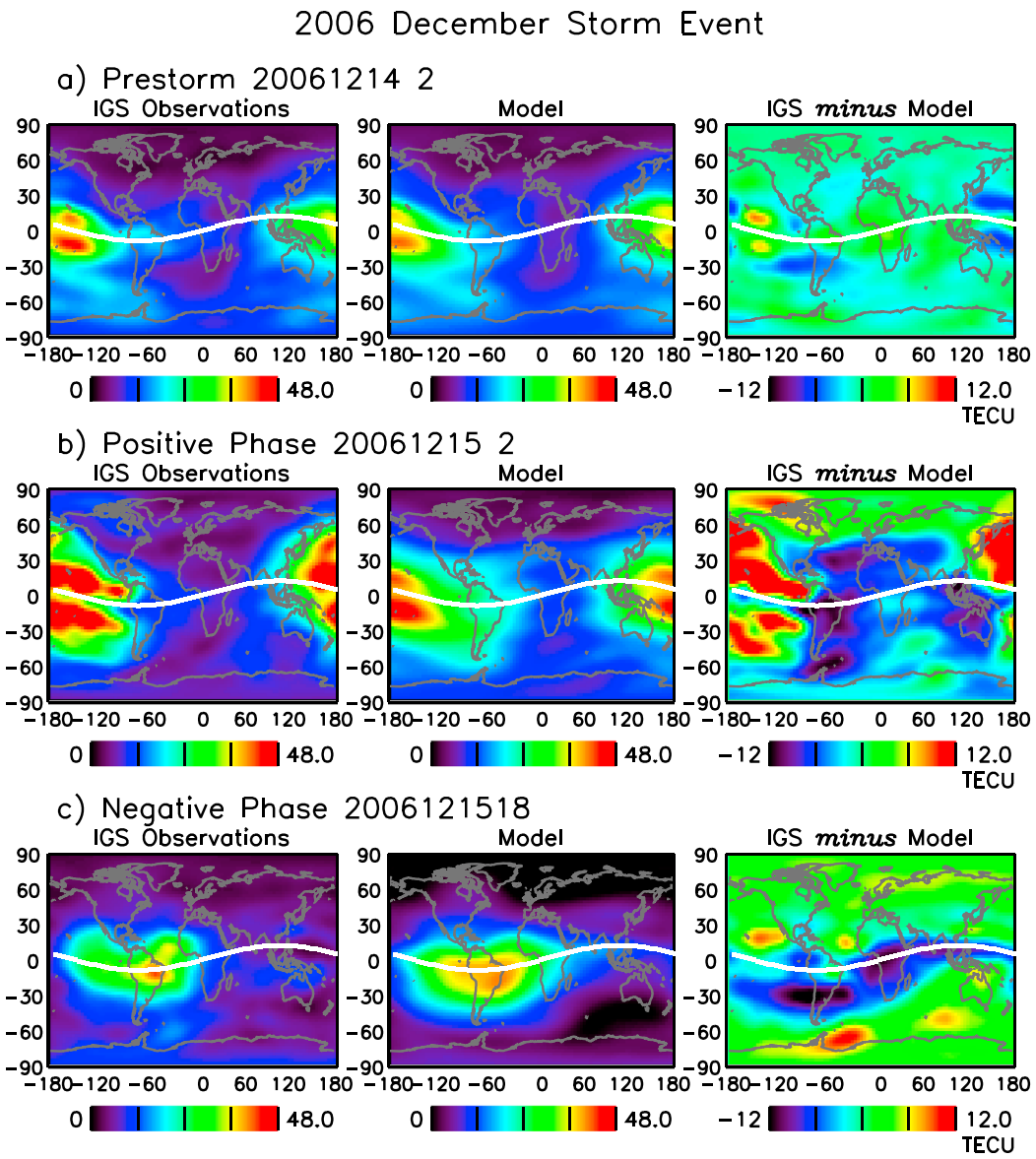

Figure 13. Compared are the IGS observations (left column) and the statistical model estimates (middle column) of regional TEC, and their differences (right column), for (a) 1 day prior to the storm at 02 UT on 14 December 2006, (b) the peak positive phase of the storm at 02 UT on 15 December 2006, and (c) the peak negative phase of the storm at 18 UT on 15 December 2006. The dashed lines in Figure 12 identify geomagnetic activity and global TEC at each of these three times. TEC = total electron content; TECU = TEC unit, 1 TECU = 10^{16} el/m^2; IGS = International Global Navigation Satellite Systems Service.

ahead, the statistical model approach does not require real-time observations, and it forecasts TEC on time scales beyond 1 day. The solar EUV irradiance input to the model is determined from an autoregressive representation of variability in the prior 100 days; the geomagnetic inputs, which are only minimally autocorrelated, are not forecast.

The MAE of the statistical model's regional TEC forecasts and IGS observations during 1999 to 2015 (the period for which the model parameters are estimated), averaged over the globe, increases from 2.5 to 3.2 TECU as the time increment of the forecast increases from $\Delta t = 1$ to $\Delta t = 10$ days; the corresponding RMSE increases from 3.7 to 4.8 TECU, and the MAPE increases from 16% to 21%. Averaged over just the low to

middle latitudes (30°S to 30°N) that encompass the EIA the $MAE_{fc}^{\Delta t}$ of the statistical model's forecasts increase from 3.2 to 4.3 TECU as the time increment of the forecast increases from $\Delta t = 1$ to $\Delta t = 10$ days; the corresponding $RMSE_{fc}^{\Delta t}$ increases from 4.6 to 6.4 TECU and the $MAPE_{fc}^{\Delta t}$ from 13% to 17%.

In the subsequent validation period (2016–2017) the metrics of the statistical model's forecasts are smaller than for the entire estimation period because average solar activity is lower in 2016–2017 than in 1999–2015. But the forecast metrics are nevertheless systematically larger than for a 2-year period (2005–2006) when solar activity is comparable to that of the validation period. For example, the MAE of the TEC forecasts at $\Delta t = 5$ days ahead (averaged over the globe) is $MAE_{fc}^{\Delta t}$ =2.7 TECU for the estimation period, 2.0 TECU for the validation period, and 1.7 TECU for 2005–2006. This suggests that forecast errors evaluated during the estimation period may underestimate the actual errors (by 10% to 40%, depending on season) when using the statistical model to forecast TEC in epochs beyond the estimation period. Robust validation of the statistical model's forecast skill awaits metrics corresponding to forecasts made over a future solar cycle of IGS TEC observations, not just 2 years at low solar activity.

The statistical model forecasts depend on solar activity, season of the year and geographical location. The MAE and RMSE metrics that quantify absolute errors of the model's forecasts compared with observations are larger when solar activity is higher; for example, $MAE_{fc}^{\Delta t}$ for the $\Delta t = 5$ day forecast increases from 1 TECU during low solar activity (2008–2009) to 4 TECU during high solar activity (2000–2001). Forecast errors are larger during April than July; the $MAE_{fc}^{\Delta t}$ of the $\Delta t = 5$ day forecast (for 1999–2015) is 3 TECU in April and 2 TECU in July. Regionally, maximum forecast errors occur at distinct locations within the EIA and at high southern latitudes, which may correspond to sites of lower metrological influences that the model does not include but that are also regions where the IGS TEC observations have largest uncertainties.

Errors in the statistical model forecasts are generally smaller than the errors in forecasts made using persistence and climatology of the IGS observations. Skill scores of the statistical model's forecasts averaged over the globe (determined using 2-hourly values in all months from 1999 to 2015) are positive relative to persistence and climatology for all forecast time increments from $\Delta t = 3$ to 10 days and are comparable at $\Delta t = 2$ days. Only for the $\Delta t = 1$-day forecasts does persistence perform better than the statistical model. And while errors in the statistical model forecasts are themselves larger, in terms of absolute TECU, in April than in July the model nevertheless performs better than both persistence and climatology in these months.

A key region where the statistical model's performance in both specifying and forecasting TEC is relatively poor is at high southern latitudes, especially in the vicinity of the Weddell Sea; here the errors in the statistical model forecasts are larger than forecasts made using persistence and climatology. This may because the IGS observations themselves have large uncertainties at high southern latitudes, due to a lack of GPS ground receivers, with the result that the model's statistical parameterizations of TEC's variability components are least certain. This region also exhibits anomalous behavior traceable of dynamical motions possibly related to influences from lower atmosphere meteorology, which the model does not include.

The statistical model forecasts are readily extended from time scales of days to months and years, given projections of the solar activity and geomagnetic activity inputs to the model. In particular, a parameterization of monthly solar EUV irradiance in terms of sunspot numbers illustrates use of the SWPC forecasts of sunspot numbers for forecasting TEC in future years. Forecasts of geomagnetic activity are currently difficult and uncertain (Mannucci et al., 2015); as they improve, their incorporation into the statistical model may enable improved forecasts of TEC during ionospheric storms. Although geomagnetic activity forecasts were not included in the forecasts of TEC, the ability of the statistical model to specify TEC changes in response to the geomagnetic storm of December 2006 was demonstrated to be comparable to eight other models—both statistical and physical—whose capabilities a community challenge recently quantified.

As the IGS database continues to lengthen, and the ability to forecast solar and geomagnetic activity advances, the performance of the statistical model forecasts can continue to be validated and improved, on multiple time scales. The metrics of the model performance evaluated for the database thus far provide a baseline for future work quantifying the capability of forecasting ionospheric TEC more than 24 hr

ahead, which is the limit of current operations. An additional prospect for improvements in forecasting TEC variations beyond the demonstrated capability of the statistical model is inclusion of lower-atmosphere meteorology.

Acknowledgments
The Chief of Naval Research funded this work. The IGS TEC database is available at the website (http://cdaweb.gsfc.nasa.gov). The Mg index used to calculate the EUV irradiance is available at the website (http://www.iup.uni-bremen.de/gome/gomemgii.html). The $F_{10.7}$ and *ap* indices are available at the website (https://www.ngdc.noaa.gov/stp/spaceweather.html). The *Dxt* index is provided by the Dcx server of the University of Oulu, Finland, at the website (http://dcx.oulu.fi). Supporting information includes an IDL procedure (NRLTEC_2hr_SW.pro) that calculates the global and regional TEC and a separate IDL procedure (NRLSSI_EUV_SW.pro) that calculates the solar EUV irradiance, which the model inputs, together with a text file (NRLTEC_input_output_data_SW.txt) of the inputs and output of NRLTEC_2hr_SW.pro and a text file (NRLSSI_EUV_input_output_data_SW.txt) of the inputs and output of NRLSSI_EUV_SW.pro for the period 1998 to 2017.

References

American Meteorological Society (2011). Satellite navigation & space weather: Understanding the vulnerability & building resilience. Policy Workshop Report.

Belehaki, A., Zolesi, B., Juren, C., Dialetis, D., Stanislawska, I., Bremer, J., et al. (2006). Monitoring and forecasting the ionosphere over Europe: The DIAS project. *Space Weather*, *4*, S12002. https://doi.org/10.1029/2006SW000270

Cannon, P. S. (2009). Mitigation and exploitation of the ionosphere: A military perspective. *Radio Science*, *44*, RS0A20. https://doi.org/10.1029/2008RS004021

Chai, T., & Draxler, R. R. (2014). Root mean square error (RMSE) or mean absolute error (MAE)?—Arguments against avoiding RMSE in the literature. *Geoscientific Model Development*, *7*(3), 1247–1250. https://doi.org/10.5194/gmd-7-1247-2014

Filler, R., Ganop, S., Olson, P., Sokolowski, S., & Fischer W. (2004). Positioning, navigation and timing: The foundation of command and control. United States Army Command and Control Directorate (Cerdec), Fort Monmouth NJ.

Fuller-Rowell, T., Araujo-Pradere, E., Minter, C., Codrescu, M., Spencer, P., Robertson, D., & Jacobson, A. R. (2006). US-TEC: A new data assimilation product from the Space Environment Center characterizing the ionospheric total electron content using real-time GPS data. *Radio Science*, *41*, RS6003. https://doi.org/10.1029/2005RS003393

Fuller-Rowell, T. J., Codrescu, M. C., & Wilkinson, P. (2000). Quantitative modeling of the ionospheric response to geomagnetic activity. *Annales Geophysicae*, *18*(7), 766–781.

Hernández-Pajares, M., Juan, J. M., Sanz, J., Orus, R., Garcia-Rigo, A., Feltens, J., et al. (2009). The IGS VTEC maps: A reliable source of ionospheric information since 1998. *Journal of Geodesy*, *83*(3-4), 263–275. https://doi.org/10.1007/s00190-008-0266-1

Jakowski, N., Mayer, C., Hoque, M. M., & Wilken, V. (2011). Total electron content models and their use in ionosphere monitoring. *Radio Science*, *46*, RS0D18. https://doi.org/10.1029/2010RS004620

Jee, G., Lee, H.-B., Kim, Y. H., Chung, J.-K., & Cho, J. (2010). Assessment of GPS global ionosphere maps (GIM) by comparison between CODE GIM and TOPEX/Jason TEC data: Ionospheric perspective. *Journal of Geophysical Research*, *115*, A10319. https://doi.org/10.1029/2010JA015432

Lean, J. L., Meier, R. R., Picone, J. M., & Emmert, J. T. (2011). Ionospheric total electron content: Global and hemispheric climatology. *Journal of Geophysical Research*, *116*, A10318. https://doi.org/10.1029/2011JA016567

Lean, J. L., Meier, R. R., Picone, J. M., Sassi, F., Emmert, J. T., & Richards, P. G. (2016). Ionospheric total electron content: Spatial patterns of variability. *Journal of Geophysical Research: Space Physics*, *121*, 10,367–10,402. https://doi.org/10.1002/2016JA023210

Lean, J. L., Woods, T. N., Eparvier, F. G., Meier, R. R., Strickland, D. J., Correira, J. T., & Evans, J. S. (2011). Solar extreme ultraviolet irradiance: Present, past, and future. *Journal of Geophysical Research*, *116*, A01102. https://doi.org/10.1029/2010JA015901

Mannucci, A. J., Verkhoglyadova, O. P., Tsurutani, B. T., Meng, X., Pi, X., Wang, C., et al. (2015). Medium-range thermosphere-ionosphere storm forecasts. *Space Weather*, *13*, 125–129. https://doi.org/10.1002/2014SW001125

Mendillo, M. (2006). Storms in the ionopshere: Patterns and processes for total electron content. *Reviews of Geophysics*, *44*, RG4001. https://doi.org/10.1029/2005RG000193

Schunk, R. W., Gardner, L., Scherliess, L., & Zhu, L. (2012). Problems associated with uncertain parameters and missing physics for long-term ionosphere-thermosphere forecasting. *Radio Science*, *47*, RS0L23. https://doi.org/10.1029/2011RS004911

Schunk, R. W., Scherliess, L., Eccles, V., Gardner, L. C., Sojka, J. J., Zhu, L., et al. (2014). Ensemble modeling with data assimilation models: A new strategy for space weather specifications, forecasts, and science. *Space Weather*, *12*, 123–126. https://doi.org/10.1002/2014SW001050

Shim, J. S., Rastätter, L., Kuznetsova, M., Bilitza, D., Codrescu, M., Coster, A. J., et al. (2017). CEDAR-GEM challenge for systematic assessment of ionosphere/thermosphere models in predicting TEC during the 2006 December storm event. *Space Weather*, *15*, 1238–1256. https://doi.org/10.1002/2017SW001649

Space Weather Action Plan (2015). US National Science and Technology Council.

Space Weather Phase I Benchmark (2017). National Science and Technology Council.

Tsagouri, I. (2011). Evaluation of the performance of DIAS ionospheric forecasting models. *Journal of Space Weather and Space Climate*, *1*, A02. https://doi.org/10.1051/swsc/2011110003

Tsagouri, I., Koutroumbas, K., & Elias, P. (2018). A new short-term forecasting model for the total electron content storm time disturbances. *Journal of Space Weather and Space Climate*, *2018*, A33. https://doi.org/10.1051/swsc/2018019

Verbanac, G., Vršnak, B., Temmer, M., Mandea, M., & Korte, M. (2010). Four decades of geomagnetic and solar activity: 1960–2001. *Journal of Atmospheric and Solar - Terrestrial Physics*, *72*(7-8), 607–616. https://doi.org/10.1016/j.jastp.2010.02.017

von Storch, H., & Zwiers, F. W. (1999). *Statistical analysis in climate research*. Cambridge, UK: Cambridge University Press.

Wilks, D. S. (1995). *Statistical methods in the atmospheric sciences*. San Diego, CA: Academic Press.

Willmott, C. J., & Matsuura, K. (2005). Advantages of the mean absolute error (MAE) over the root mean square error (RMSE) in assessing average model performance. *Climate Research*, *30*, 79–82. https://doi.org/10.3354/cr030079

Wood, B. E., Lean, J. L., McDonald, S. E., & Wang, Y.-M. (2016). Comparative ionospheric impacts and solar origins of nine strong geomagnetic storms in solar cycle 24, 2010–2015. *Journal of Geophysical Research: Space Physics*, *121*, 4938–4965. https://doi.org/10.1002/2015JA021953